AD-A143 591 AN EXPERIMENTAL STUDY OF THE TRANSONIC EQUIVALENCE RULE WITH LIFT PART 2 (.. (U) NATIONAL AERONAUTICAL ESTABLISHMENT OTTAWA (ONTARIO) HIGH SPE.. Y Y CHAN 1/1

UNCLASSIFIED MAR 84 NAE-LR-614-PT-2 NRC-23412 F/G 20/4 NL

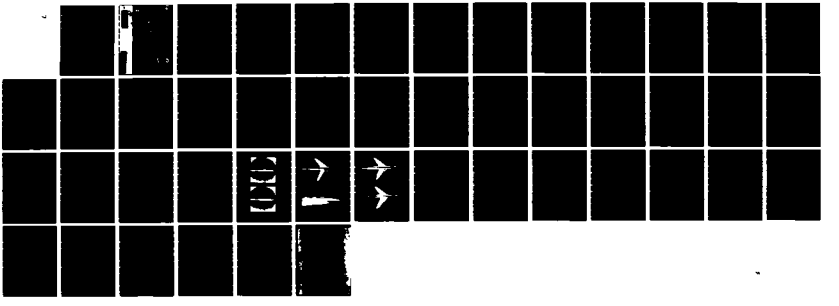

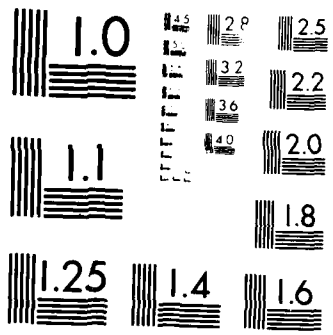

National Research Council Canada
Conseil national de recherches Canada

AN EXPERIMENTAL STUDY OF THE TRANSONIC EQUIVALENCE RULE WITH LIFT

PART II

by

Y.Y. Chan

National Aeronautical Establishment

OTTAWA
MARCH 1984

Canada

AERONAUTICAL REPORT
LR-614
NRC NO. 23412

NATIONAL AERONAUTICAL ESTABLISHMENT

SCIENTIFIC AND TECHNICAL PUBLICATIONS

AERONAUTICAL REPORTS:

Aeronautical Reports (LR): Scientific and technical information pertaining to aeronautics considered important, complete, and a lasting contribution to existing knowledge.

Mechanical Engineering Reports (MS): Scientific and technical information pertaining to investigations outside aeronautics considered important, complete, and a lasting contribution to existing knowledge.

AERONAUTICAL NOTES (AN): Information less broad in scope but nevertheless of importance as a contribution to existing knowledge.

LABORATORY TECHNICAL REPORTS (LTR): Information receiving limited distribution because of preliminary data, security classification, proprietary, or other reasons.

Details on the availability of these publications may be obtained from:

Publications Section,
National Research Council Canada,
National Aeronautical Establishment,
Bldg. M-16, Room 204,
Montreal Road,
Ottawa, Ontario
K1A 0R6

ÉTABLISSEMENT AÉRONAUTIQUE NATIONAL

PUBLICATIONS SCIENTIFIQUES ET TECHNIQUES

RAPPORTS D'AÉRONAUTIQUE

Rapports d'aéronautique (LR): Informations scientifiques et techniques touchant l'aéronautique jugées importantes, complètes et durables en termes de contribution aux connaissances actuelles.

Rapports de génie mécanique (MS): Informations scientifiques et techniques sur la recherche externe à l'aéronautique jugées importantes, complètes et durables en termes de contribution aux connaissances actuelles.

CAHIERS D'AÉRONAUTIQUE (AN): Informations de moindre portée mais importantes en termes d'accroissement des connaissances.

RAPPORTS TECHNIQUES DE LABORATOIRE (LTR): Informations peu disséminées pour des raisons d'usage secret, de droit de propriété ou autres ou parce qu'elles constituent des données préliminaires.

Les publications ci-dessus peuvent être obtenues à l'adresse suivante:

Section des publications
Conseil national de recherches Canada
Établissement aéronautique national
Im. M-16, pièce 204
Chemin de Montréal
Ottawa (Ontario)
K1A 0R6

AN EXPERIMENTAL STUDY OF THE TRANSONIC EQUIVALENCE RULE WITH LIFT

PART II

ÉTUDE EXPÉRIMENTALE DE L'APPLICATION À LA PORTANCE DE LA RÈGLE D'ÉQUIVALENCE TRANSSONIQUE

PARTIE II

by/par

Y.Y. Chan

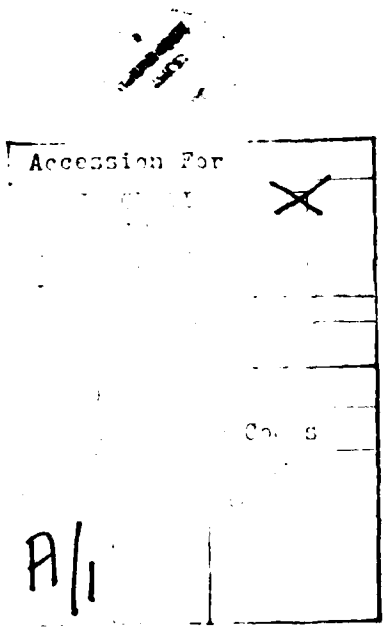

L.H. Ohman, Head/Chef
High Speed Aerodynamics Laboratory/
Laboratoire d'aérodynamique à hautes vitesses

G.M. Lindberg
Director/Directeur

SUMMARY

The experimental study of the transonic equivalence rule with lift, previously reported in Reference 1, has been extended to include a configuration of swept-back wing-body and the corresponding equivalent bodies for lift and zero-lift. For zero lift, the wing-body is shown to have higher wave drag than that of the equivalent body. At lifting condition, the analyses of the data, including those of the delta wing-bodies reported in Reference 1, have verified the similitude of drag rise due to lift between the wing-bodies. The additional drag induced by the effective area due to lift on the equivalent body was found to agree reasonably with the wave drag generated by lift on the wing-body. The experiment thus verified the area rule with lift which must be considered in the optimal design of transonic configurations.

RÉSUMÉ

L'étude expérimentale de la loi de l'équivalence transsonique pour la portance, précédemment signalée dans la référence 1, a été élargie pour inclure le profil alaire à flèche et les corps équivalents correspondants pour la portance et la portance nulle. Pour la portance nulle, il a été démontré que le profil alaire présente une traînée d'onde supérieure à celle du corps équivalent. En condition de portance, les analyses de données, y compris celles des profils alaires delta signalés dans la référence 1, ont confirmé la similitude de l'augmentation de traînée causée par la portance entre les divers profils alaires. La traînée additionnelle induite par la surface réelle en raison de la portance produite sur un corps équivalent s'accordait raisonnablement à la traînée d'onde créée par la portance sur le profil alaire. L'expérience a ainsi confirmé la loi des aires pour la portance, laquelle doit être prise en compte dans la conception optimale des profils transsoniques.

CONTENTS

TABLES

ILLUSTRATIONS

ILLUSTRATIONS (Cont'd)

APPENDIX

SYMBOLS

Symbol	Definition
a	leading edge contour of the wing planform, Equation (A1)
A	aspect ratio of the wing, Equation (11)
b	semi-span of the wing, Equation (1)
c_0	reference length = total length of gross wing planform, Equation (1)
C_D	drag coefficient, Figure 5
$\bar{C}_D$	$C_D - C_{D_m}$
C_{D_c}	drag coefficient based on maximum cross-sectional area, Figure 6
C_{D_i}	induced drag coefficient, Equation (11)
C_{D_m}	minimum drag coefficient
C_{D_w}	wave drag coefficient, Equation (13)
ΔC_{D_c}	drag differential of equivalent bodies, Figure 18
C_L	lift coefficient
$\bar{C}_L$	$C_L - C_{L_m}$, Figure 5
C_{L_m}	C_L at C_{D_m}
$\bar{C}_{L_{\bar{\alpha}}}$	local lift curve slope
$\bar{C}_{L_{\bar{\alpha}_0}}$	lift curve slope at zero lift, Figure 10
ΔD_w	wave drag rise, Equation (14)
k	induced drag factor, Equation (11)
k_v	vortex drag factor, Equation (12)

SYMBOLS (Cont'd)

Symbol	Definition
k_w	wave drag factor, Equation (13)
K	transonic similarity parameter for equivalent body, Figure 6
K_t	transonic similarity parameter based on wing thickness, Figure 10
ℓ	body length, Equation (10)
M_∞	free stream Mach number
q	free stream dynamic pressure, Equation (14)
S_c	geometric cross-sectional area, Equation (10)
S_e	effective cross-sectional area, Equation (10)
S_w	wing area, Table 2
t	maximum thickness of wing section
x,y,z	Cartesian co-ordinates
$\bar{x}$	x/c_0, Equation (10)
$\tilde{x}$	x/ℓ, Equation (10)
α	angle of attack
$\bar{\alpha}$	$\alpha - \alpha_m$
α_m	α at C_{D_m}
$\tilde{\alpha}$	angle of attack parameter, Equation (10)
γ	ratio of specific heat, Equation (10)
$\tilde{\epsilon}$	ratio of transverse length scales, Equation (10)
λ	wing sweep parameter with respect to the reference length C_0, Equation (10)
$\tilde{\lambda}$	wing sweep parameter with respect to the body length
$\tilde{\tau}$	body thickness parameter, Equation (10)
τ_b	slender ratio of equivalent body, maximum diameter/ℓ, Figure 6
ϕ	velocity potential, Equation (2)

AN EXPERIMENTAL STUDY OF THE TRANSONIC EQUIVALENCE RULE WITH LIFT

PART II

1.0 INTRODUCTION

In a previous report (Ref. 1) an experimental investigation of the transonic area rule with lift was presented. The purpose of the experiment was to examine the validity of the theoretical results on the extension of the classical area rule with lift[2]. The extended rule is given in a form of flow similitude. It states that the flows are equivalent if the distributions of sources $S_e'(x)$ and the doublets $D_o(x)$ along the body axis are identical for the same transonic similarity parameter based on the maximum cross-sectional area of the configurations. The sources are related to the geometry of the body and its effective enlargement due to lift, and the doublets to the lift disttribution along the configuration. The effective cross-sectional area due to lift has been shown to be appreciable and induces additional wave drag in the transonic flight range[3].

This early investigation was concerned with two delta wing-body combinations whose drag characteristics were determined at transonic speeds. The models had the same cross-sectional area distribution but different wing span and thickness. The equivalent bodies for zero lift and for a specified lift were also included in the investigation. The delta wing was chosen because the planform shape allowed the design of identical effective cross-sectional areas due to lift for models with different swept-back parameters. However, most of the transonic aircraft have swept-back wing with moderate or large aspect ratios. From a practical point of view, it is essential to evaluate the applicability of the extended area rule to such a configuration. A swept-back wing-body model was thus designed to be investigated in the transonic Mach number range as in the previous experiment. The geometric and aerodynamic parameters of the swept wing model were designed to be closely to those of the delta wing, so that the data from both experiments could be compared directly.

In the delta wing experiment, the wave drag and induced drag due to lift were correlated to the square of lift and the inverse of lift curve slope. For a thin wing without leading edge suction, the induced drag factor, henceforth called drag factor, defined in this manner would approach unity[4]. For the delta wings with round leading edges, the drag factors ranging from 0.6 to 0.8 were obtained. Based on the drag factor defined in such manner, the wave drag of the delta wing due to lift was deduced and the results for two wings were found to be closely similar throughout the Mach number range studied. The inclusion of the lift curve slope in the drag-lift correlation, however, is later found to be less desirable as the former varies appreciable in the transonic range. The drag factor defined in such a manner will no longer be a simple correlation function of the drag-lift polar at a given Mach number. An alternative approach is to replace the experimental lift curve slope by its theoretical slender wing value of $\pi A/2$, where A is the aspect ratio. The drag factor is then in its conventional form and depends only on the drag-lift correlation at a given Mach number. The data of the delta wings in Reference 1 and the present data of the swept wing are analyzed in this report using this form of the drag factor. The wave drag due to lift is also deduced in this form. The results of all three wing-bodies are then presented together for comparison.

In what follows, the model design and the aerodynamic consideration of the swept wing-body will be first presented. The experimental results and their analyses, including the data of the delta wing-bodies, are then given in detail and related to the extended equivalence rule with lift. The basic concepts of the theory can be found in Reference 1 and will not be repeated herein.

2.0 DESIGN OF THE SWEPT WING-BODY MODELS

2.1 Geometrical Design

The swept wing-body has a cylindrical central body similar to that of the delta wing-body Model WB2. The span, the aspect ratio and the angle of sweep of the leading edge of the swept wing

are taken to be the same as those of the delta wing Model WB2 before the wing tip round off (Fig. 1). The mean aerodynamic chord is chosen to be three inches so that the wing area will be close to that of WB2. The wing has a taper ratio of 0.4 and the same symmetric Boerstoel profile as that of the delta wings. The thickness to chord ratio of the section is constant along the span and there is no wing twist. The thickness of the wing is determined by matching the cross-sectional area distribution from the wing tip forward as close as possible to that of the delta wing models. The resulting area distribution for t/c = 0.057 is shown in Figure 2. The additional area at the rear of the hump comes from the outer portion of the swept wing downstream from the leading edge of the wing tip. Reduction of the additional area to fit the area contour of the delta wing cannot be achieved without altering the geometrical layout of the planform. It is preferable, however, to keep the planform characteristics of the swept wing close to those of the WB2 wing for aerodynamic consideration, thus no further modification is done to the cross-sectional area distribution. The resulting equivalent body is thus not exactly identical to that for the delta wing. The complete body shape is shown in Figure 1 as Model BS1. The wing tip is rounded off to ease the local spanwise loading and the adverse effects due to sweep[5]. The wing tip contour is designed to be

$$\frac{y}{b} = 0.2 \sin\left[\frac{x/c_0 - 0.8}{0.2}\right] \qquad \begin{matrix} x/c_0 \geqslant 0.8 \\ y/b \geqslant 0.8 \end{matrix} \tag{1}$$

where b is the semi-span and the reference length c_0 is that of the delta wing model, taken as a scale for the present wing design.

The basic dimensions and the nondimensional parameter of the final design for the wing-body model are given in Table 1. The parameters of the wing sweep $\tilde{\lambda}$ and the thickness $\tilde{\tau}$ have values only slightly different from those of the delta wing Model WB2. the product of these parameters $\tilde{\lambda}\,\tilde{\tau}$ is nearly identical for both models. Some of these geometrical parameters, which are important for the correlations of the experimental data, are listed in Table 2 for both the swept wing and the delta wing models.

2.2 Aerodynamic Design

When the wing-body is at lifting condition, the flow about the configuration is governed by the effective sources and doublets distributed along the body axis. The strengths of these singularities are given explicitly in terms of three functions F(x), E(x) and T(x) depending on the load distribution of the wing[1,2]. For the present planform, the load distribution is unknown and has to be determined experimentally or theoretically. However, it is noted that these functions are not too sensitive to the details of load distribution for a given planform. An approximate expression of the load distribution reflecting all essential characteristics of the wing loading has been shown to be adequate[3]. The expression for load distributions given in Reference 3 is adopted herein. The jump of the velocity potential across the wing plane can be written as follows,

$$\| \phi \| = \frac{(x - x_\ell)^{3/2}}{(x_t - x_\ell)^{3/2}} \left[a_0 + a_1 (x_t - x) + a_2 (x_t - x)^2 + \ldots \right] \tag{2}$$

$$\text{for} \quad x_\ell < x < x_t$$

where the subscripts ℓ and t denote the leading and the trailing edges respectively. The wing loading is given by the x-derivative of the potential jump and thus gives a square root decay of loading as the leading edge is approached. The coefficients in the polynomial are determined by the conditions at the trailing edge at which it is assumed that the spanwise loading is elliptical and the chord-wise loading decays linearly. In the wake the load is zero. These conditions yield respectively

$$a_0 = \frac{2}{\pi} (1 - y^2)^{1/2}$$

$$a_1 = \frac{3}{2}\,\frac{a_0}{x_t - x_\ell}$$

$$a_2 = 0 \tag{3}$$

With the conditions at the trailing edge specified, the potential jump can be written as

$$[\![\,\phi\,]\!] = \frac{1}{\pi}\,(1-y^2)^{1/2}\,\frac{(x-x_\ell)^{3/2}}{c^{5/2}}\,\left[5(x_t - x) + 2(x - x_\ell)\right] \tag{4}$$

where $c = x_t - x_\ell$, is the local chord. The x and y derivatives of the potential jump are given as

$$[\![\,\phi_x\,]\!] = \frac{15}{2\pi c^{5/2}}\,(1-y^2)^{1/2}\,(x-x_\ell)^{1/2}\,(x_t - x) \tag{5}$$

$$[\![\,\phi_y\,]\!] = [\![\,\phi\,]\!]\left[-\frac{y}{1-y^2} - \frac{5}{2}\,\frac{1}{c}\,\frac{dc}{dy} - \frac{3}{2}\,\frac{1}{x-x_\ell}\,\frac{dx_\ell}{dy} + \frac{5\dfrac{dx_t}{dy} - 2\dfrac{dx_\ell}{dy}}{5(x_t - x) + 2(x - x_\ell)}\right] \tag{6}$$

At the wake trailing behind the wing, the conditions in Equation (3) give

$$[\![\,\phi\,]\!] = \frac{2}{\pi}\,(1-y^2)^{1/2} \tag{7}$$

$$[\![\,\phi_x\,]\!] = 0 \tag{8}$$

$$[\![\,\phi_y\,]\!] = -\frac{2}{\pi}\,\frac{y}{(1-y^2)^{1/2}} \tag{9}$$

matching continuously with the expressions in Equations (4), (5) and (6) at the trailing edge. It should be noted that the spatial variables x and y in this section (and in the Appendix) have been scaled by the total length c_0 and the semi-span b of the wing planform respectively. With the load distribution specified, the functions F(x), E(x) and T(x) are evaluated numerically. Some details of the numerical procedure are given in the Appendix. The results are shown in Figure 3 with the abscissa scaled by the planform length c_0, so that a direct comparison with the delta wing case can be made. For the swept wing, the x-derivative of the function F(x), $F_x(x)$, relating to the axial load distribution, peaks at about the mid point of the planform length, while on the delta wing, it reaches a maximum near the trailing edge. The function T(x), relating to the load distribution over the wing surface, behaves similarly for both planforms. The function E(x) signifies the cross-flow kinetic energy and has the same trend for both cases.

The design conditions for the lifting case are the same as those of the delta wing,

$$M_\infty = 0.975$$

$$\tilde{\epsilon} = 0.0711$$

$$\frac{\tilde{\epsilon}\,\tilde{\alpha}}{\tilde{\tau}} = 0.2024$$

The effective area due to lift can now be calculated from the expression (Eq. (25) of Ref. 1) for the wing body.

$$\tilde{S}_e(\tilde{x}) - \tilde{S}_c(\tilde{x}) = \frac{1}{2}\left(\tilde{\epsilon}\frac{\tilde{\alpha}}{\tilde{\tau}}\right)^2\left(\frac{\ell}{c_0}\right)^2\left[\frac{2\,|\ell n\,\tilde{\epsilon}\,|+1}{8\pi}\,F_\lambda^{\,2}(\bar{x}) + T(\bar{x}) + \frac{2}{(\gamma+1)\lambda^2}\,E(\bar{x})\right] \tag{10}$$

where the tilded x is scaled by the body length ℓ and the barred x by the planform length c_0. The resulting effective area is shown in Figure 4. The area distribution for the delta wing is also shown for comparison. Because of the nearly symmetrical form of the loading functions $F_\lambda(\bar{x})$ and $T(\bar{x})$ for the swept wing, the effective area is more evenly distributed at both sides of the peak, while for the delta wing the distribution is highly weighted towards the trailing edge. With the effective area due to lift added to the basic geometric cross-sectional area $S_c(x)$, the final area distribution of the equivalent body for the lifting case is shown in Figure 2. The corresponding model, designated BS2, is shown in Figure 1. Note that the nose piece is common for all models.

3.0 EXPERIMENTAL RESULTS AND DISCUSSIONS

3.1 Experimental Program

The experiments were performed in the transonic test section of the NAE 5-ft (1.5 m) × 5-ft (1.5 m) blowdown wind tunnel. The experimental set-up was similar to that of the delta wing investigation. The forces and moments of the model were measured by a one inch Able MK22 6-component internal balance. The base pressure was also measured to complement the balance drag measurements. The static pressure distribution along the top and bottom walls were monitored by one inch static pressure pipes. Boundary layer transitions on the wings and the nose of the body were left free as in the delta wing experiments. Surface flow visualizations were obtained for certain Mach numbers and angles of attack. Schlieren visualizations of the flow field were also taken for cases with Mach number close to unity. The test Mach number ranged from 0.8 to 1.1. The Reynolds number was fixed at 8×10^6 per foot or 2×10^6 based on the mean aerodynamic chord of the swept wing model. The raw data were reduced by the same computer program as used for the delta wing investigation. The results are presented in terms of $\bar{C}_L$, $\bar{\alpha}$ and C_D in Figure 5 for the wing-body Model WBS. The same data are also listed in Table 3. These data are further analyzed in terms of parameters of the equivalence rule and compared directly with those of the delta wing models.

3.2 Drag at Zero Lift

The transonic drag rises for the wing-body Model WBS and the equivalent body BS1 are shown in Figure 6. The drag rise of the swept wing Model WBS follows closely to that of the delta wing Model WB2 up to a value of K, the similarity parameter of about - 1.0, corresponding to a Mach number of 0.98. At higher Mach numbers, the wave drag of the swept wing model increases steadily and is higher than those of the delta wing models.

For a swept wing with moderate aspect ratio and sweep-back angle, the flow about the wing retains some two-dimensional sectional characteristics and at high Mach numbers shocks with nearly constant strength extend along the full span. This shock formation can be seen from the Schlieren flow visualizations, a typical one shown in Figure 7, taken at a Mach number of 0.98, shows an oblique shock at the trailing edge turning rapidly normal to the flow. For a delta wing, the flow about the wing is more three-dimensional and nearly conical, thus the shock decays along the span. The surface flow visualization in Figure 8 shows, at the outer portion of the swept wing, that the shock interacts strongly with the boundary layer causing local flow separation. The strong shock and the flow separation on the swept wing may contribute to the higher drag in comparison with the delta wing.

The drag rise of the equivalent body for the swept wing-body BS1 is also shown in Figure 5. For Mach number less than unity, the drag rise of BS1 is about half of that of WBS, although the general shape of these two curves are closely similar over the range of the Mach number considered. The same discrepancy has been observed in the original area rule study[6] and in more recent experiments[7,8]. The Schlieren picture of BS1 in Figure 7 shows a near normal shock formed not far from the end of the hump. The shock decays faster than that of the WBS and thus is weaker. The surface flow visualization indicates no boundary layer separation at the aft portion of the hump (Fig. 8).

Figure 6 also shows that the drag rise of BS1 is appreciably lower than that of B1, the equivalent body for the delta wing models. Comparison of the Schlieren pictures of BS1 in Figure 7 and that for B1 in Figure 9 of Reference 1 clearly indicates that the gradual reduction of the hump at the downstream side helps to weaken the shock. It may be recalled that the body contour ahead of the maximum cross-section is practically identical for both models.

For the far field, the data of the static pressure distributions along the upper and the lower walls are found to be too scattered for analysis to establish flow similarity. Thus no study of the far field similarity was made for the swept wing model and its equivalent bodies.

3.3 Lift

The lift versus angle of attack curves for all test Mach numbers are plotted in Figure 5. Slight nonlinearity of the lift curve above two degrees angle of attack can be observed for all cases especially for those between Mach number 0.9 to 1.0. The nonlinear increase of lift has been shown to be due to the tip vortex sheet, which induces a vortex lift, usually associated with slender delta wings[9]. Another significant aerodynamic chracteristic of the swept wing observed in the experiment is the strong upwash over the outer portion of the wing, induced by the spanwise component of the trailing vorticity shedded from the wing[10]. This effective incrase of angle of attack along the span causes the formation of a strong shock and flow separation at the outer portion of the wing, which can be clearly seen from the surface flow visualization (Fig. 9). At 2.9 degree angle of attack for instance, trailing edge separation starts from the wing tip and spreads inward to about one-third of the wing span. Strong shock-boundary layer interaction is indicated by the rapid turning of the surface streamline at the separation region. Stronger interaction can be seen as the angle of increase to 5.5 degree. The S shape of surface streamlines at the mid portion of the wing indicates the formation of a second shock ahead of the main shock at the inner portion of the wing, the existence of which has been shown both experimentally and theoretically[11,12].

The lift curve slopes at zero lift are correlated against the transonic similarity parameter based on the wing thickness in Figure 10. The delta wing cases are also shown for comparison. The present data show a small rise between Mach numbers of 0.92 to 0.96 with a peak at 0.94. The rest of the data vary only slightly through the Mach number range. The values at both the subsonic and supersonic ends approach those of the delta wing WB1. At the low Mach number end, the values of $\bar{C}_{L_\alpha}/A$ agree well with that predicted by subsonic linear theory[13]. At Mach number unity, the transonic correlation of $\bar{C}_{L_\alpha}(t/c)^{1/3}$ versus $A(t/c)^{1/3}$ is close to that of the delta wing WB2[14].

3.4 Induced Drag

Before the wave drag becomes appreciable, the drag force acting on the wing-body is composed of the induced drag due to lift, the skin friction and the pressure drag caused by boundary layer displacement or separation. The latter two components can be identified as viscous drag as they exist only in viscous flows. At zero lift, the total drag consists of the viscous drag only. With the viscous drag at zero incidence subtracted, the drag coefficient is plotted against the square of lift coefficient for Mach number 0.8 in Figure 11. The upper and the lower limits of the induced drag, corresponding to zero and full leading edge suction respectively, are also shown in the graph. The delta wing results from the previous experiments are also plotted for comparison. The drag polar of the swept wing is slightly lower than that of the delta wing WB2, indicating that the planform shape has only a small effect on the induced drag of these two wings having nearly the same aspect ratio. The parabolic drag polar is linear up to $\bar{C}_L{}^2$ about 0.1, above which the viscous drag is anticipated and the correlation becomes nonlinear. The classical expression for induced drag as a function of lift and aspect ratio can be written for the linear portion of the drag polar as

$$C_{D_i} = k \frac{\bar{C}_L{}^2}{\pi A} \tag{11}$$

where k is the induced drag factor. The coefficients of the parabolic relation has been obtained by a polynomial fit of the data and the coefficient of the second degree term yields $k/\pi A$. This form is used in the present analysis in preference to $\tilde{k}/\bar{C}_{L_{\bar{\alpha}}}$ employed in Reference 1. The latter involves the lift curve slope $\bar{C}_{L_{\bar{\alpha}}}$ which varies appreciably in the transonic range, thus the drag factor $\tilde{k}$ is no longer a simple coefficient of drag-lift correlation.

As the Mach number increases, the wave drag sets in. The wave drag due for lift, as well as the induced drag, is related to the square of the lift force[15]. The expression in Equation (11) can therefore be used for both the induced drag, also called vortex drag, and the wave drag, with the coefficient k containing both components. The variation of k against Mach number for the swept wing and the delta wings are shown in Figure 12. At the low Mach number end, the contribution comes solely from the vortex drag. For the delta wings WB1 has a lower induced drag factor than WB2, which has a larger aspect ratio. This may be caused by the higher suction generated by the thicker wing section of the WB1 model. As the Mach number increases, the drag factor for the WB1 model increases to a maximum and then drops sharply to a level as low as that before the drag rise. For WB2, the drag factor peaks at about the same Mach number of 0.96, drops slightly and then increases gradually as the flow becomes supersonic. The swept wing WBS has the lowest value of k before drag rise. However, it also has the highest value after drag rise. Before the drag rise, both WB2 and WBS show a dip of drag factor implying a reduction of vortex drag. This slight reduction of drag is caused by favourable interference between the wing and the body of certain configurations and has been observed in other tests of wing-body configurations[7,16].

3.5 Drag Rise of Equivalent Bodies with Lift

The transonic drag rise of the equivalent body of revolution for zero lift of the swept wing configuration BS1 has been discussed in Section 3.2. It was shown in Figure 6 that the drag rise of BS1 is much lower than that for the wing-body Model WBS. The drag rise characteristics of the equivalent body BS2, with the effective area due to lift forming a bigger bulge, would be expected to be similar. This indeed is the case when both data are plotted in terms of the similarity parameters for axisymmetrical bodies as shown in Figure 13. The data are well coalesced even though these two bodies are not exactly geometrically similar. The data of the equivalent bodies for the delta wing-bodies, B2 and B1, with and without lift respectively are also shown in the same figure. Again, the data are well correlated. The lower drag rise of the BS1, BS2 bodies in comparison with the B1, B2 bodies is due to broadening of the hump on the formers (see Fig. 2) that allows a more gentle recompression at the rear of the hump. The resulting rear shock is comparatively weaker than that of the B1, B2 bodies and no boundary layer separation has been observed on the BS1, BS bodies.

4.0 LIFT DEPENDENT WAVE DRAG OF THE SWEPT WING AND DELTA WING-BODIES

The lift depending wave drag which is the centre of the present study will be analyzed in this section. The data for the delta wing-bodies from Reference 1 will also be considered, together with the present swept wing-body data.

4.1 Correlations of the Drag Rise of the Wing-bodies

The wave drag at lifting condition can be deduced by subtracting the vortex drag portion from the total drag. Since the vortex drag does not change with Mach number, its value at Mach number 0.8, the lowest Mach number of the experiment, is taken to be the vortex drag. No wave drag is present at this Mach number. The wave drag factor is therefore

$$k_w = k - k_v \tag{12}$$

where k_v is the vortex drag factor and k_w the wave drag factor. The wave drag data is now expressed in the same form as the vortex drag in terms of lift and aspect ratio as

$$C_{D_w} = k_w \frac{\bar{C}_L^{\,2}}{\pi A} \tag{13}$$

The resulting wave drag factor for the swept wing and the delta wing-bodies are shown in Figure 14. It should be noted that the drag coefficient in Equation (13) is based on the gross wing area.

Since the lift is mainly carried by the wing, the scaling length for the drag rise due to lift should therefore be the overall chord c_0 of the wing planform[17]. The wave drag rise written in terms of the drag coefficient C_{D_w} based on wing area is thus

$$\frac{\Delta D_w}{q c_0^{\,2}} = \frac{4 C_{D_w}}{A \tilde{\tau}^2 \left(\frac{c_0}{\ell}\right)^2 \left(\frac{\ell^2}{S_c}\right)^2} \tag{14}$$

where S_c is the maximum cross-sectional area of the model. Substituting the wave drag coefficient in th .orm of Equation (13) from the experimental data into Equation (14), the drag rise takes the following form

$$\frac{\Delta D_w}{q c_0^{\,2}} = \frac{4 k_w}{A \tilde{\tau}^2 \left(\frac{c_0}{\ell}\right)^2 \left(\frac{\ell^2}{S_c}\right)^2} \frac{\bar{C}_L^{\,2}}{\pi A} \tag{15}$$

The expression can be further written in terms of the lift parameter $\tilde{\epsilon} \frac{\tilde{\alpha}}{\tilde{\tau}}$, which control both the source and the doublet strength due to lift (see Eq. (10) and Eqs. (12), (13) of Ref. 1),

$$\frac{\Delta D_w}{q c_0^{\,2}} = \left(\frac{k_w}{\tilde{\lambda}^2 \left(\frac{c_0}{\ell}\right)^2 \left(\frac{\ell^2}{S_c}\right)^2} \right) \frac{1}{4\pi(\gamma + 1) M_\infty^2 \, (\tilde{\tau}\tilde{\lambda})} \left(\tilde{\epsilon} \frac{\tilde{\alpha}}{\tilde{\tau}} \right)^2 \tag{16}$$

Since all wing-body models have the same maximum cross-sectional area, thus $\tilde{\tau}\tilde{\lambda}$ is the same for all cases. If the drag rise is directly related to the lift parameter, then the correlation of the wave drag factor as shown in the bracket of Equation (16) must be a function of Mach number only. The correlations in such form for the data of three models as a function of Mach number are shown in Figure 15. The data for the swept wing Model WBS and the delta wing Model WB2 collapse well through the whole Mach number range. These two models have nearly the same span but different root chords and planform shapes which seem to have little effect on the correlation.

The wave drag factor for the delta wing Model WB1 with a short span does not follow the correlations of the other models below Mach number 0.98. The correlation has much higher values than the other data. For Mach number greater than 0.98, the correlation drops to the same level as the others and then tends to increase again at the end of the experimental reach number range. This shows that the drag rise for wings with different spans cannot be compared for the same lift parameter in which the lift is scaled by the total planform length. It would be more appropriate in the drag rise region if the lift is caled by the span. This form is readily given by Equation (15) and the wave drag factor correlated in such a manner is shown in Figure 16. The data of the delta wing WB1 now coalesce much better in the drag rise region with the data of the other two wings with larger spans. This correlation implies that the drag rise due to lift is directly related to $\bar{C}_L{}^2/A$ in a form similar to that of the vortex drag.

From the Schlieren flow visualization taken during the experiment, the distinct characteristics of the flow with respect to these two regions of correlation can be observed. At the drag rise region, the shock waves formed about the wing are situated ahead of the trailing edge. The strength of the shock for this type of transonic flow, with a supersonic pocket terminated by a shock, depends strongly on the sectional characteristics of the wing. The dependency on the sectional geometry can be readily seen from the fact that for the present models having the same cross-sectional area, the correlation factor $A\tilde{\tau}^2$ in Equation (15) can be shown to be proportional to the mean thickness of the wing. As the Mach number increase to 0.98 and above, the shock moves to the trailing edge and the flow over the wing is fully supersonic except at a small region around the leading edge. The characteristic of the wave drag is then changed and follows the classical results of wave drag for supersonic flow.

It may be recalled that the wing-body WB1 is designed to have the same effective cross-sectional area due to lift as the Model WB2 by manipulating the special relations of the lifting function F, T and E for the delta planform so that the flow similitude may be established (see Eq. (10) and also Section 3.1 of Ref. 1 for details). The similitude of flow field does seem to exist for the far field as shown in Figure 21 of Reference 1. However, the similitude of drag rise in the form of Equation (16) does not seem to be applicable and the alternative form Equation (15), should be used.

We may now summarize the conditions of application of the area rule with lift. For configurations with nearly the same sweep-back parameter $\tilde{\lambda}$, the drag rise is directly related to the square of the lift parameter $\tilde{\epsilon}\frac{\tilde{\alpha}}{\tilde{\tau}}$. For configurations with large difference in $\tilde{\lambda}$, the drag rise is correlated to the square of the lift coefficient and the aspect ratio as $\bar{C}_L{}^2/A$. When the flow over the wing is supersonic, the lift parameter $\tilde{\epsilon}\frac{\tilde{\alpha}}{\tilde{\tau}}$ should be used regardless of the value of $\tilde{\lambda}$. The planform shape has only minor effect on the drag rise.

4.2 Comparison with Equivalent Bodies

The drag rise of the equivalent body at zero lift has been shown to be much lower than that of the wing-body for the swept wing experiment (Section 3.2). A direct comparison of the drag rise of the equivalent body including lift with the wing-body at lifting condition will therefore not be meaningful. However, the differential of the drag rise between these two equivalent bodies is caused by the additional effective area due to lift. Thus a comparison of the drag rise differential due to lift as given in the preceeding section is justified and will provide an assessment of the range of application

of the theory. For comparison, the drag rise is now given in terms of the drag coefficient based on the maximum cross-sectional area, which is the same for the wing-bodies and the equivalent body without lift. For the wing-body the drag rise is calculated from the experimental correlations given in Figures 15 and 16 at the design lift condition with $\tilde{\epsilon}\frac{\tilde{\alpha}}{\tilde{\tau}}$ equal to 0.2024.

For the swept wing-body the comparison is shown in Figure 17. The drag rise differential agrees very well with the drag rise to lift for Mach number below 0.96. For Mach number greater than 0.96, the drag rise due to lift of the wing-body is lower than the drag rise differential of the equivalent bodies. A similar comparison for the delta wing models is given in Figure 18. For the Model WB1, the drag rise up to Mach number of 0.96 is evaluated with $\bar{C}_L{}^2/A$ equal to 0.0078 corresponding to $\tilde{\epsilon}\frac{\tilde{\alpha}}{\tilde{\tau}}$ of 0.0829. For the Model WB2, the value of $\bar{C}_L{}^2/A$ yields $\tilde{\epsilon}\frac{\tilde{\alpha}}{\tilde{\tau}}$ of 0.2024 the design value. If the drag rise is compared with the same $\tilde{\epsilon}\frac{\tilde{\alpha}}{\tilde{\tau}}$ in this region, the drag curves will look like the wave drag factor curves in Figure 15. The comparison in Figure 18 shows that for delta wings the equivalent body differential gives a much higher drag rise than that generated by lift. However, it should be noted that flow separation occurs at the rear of the hump of the equivalent body with lift, B2 at the higher Mach numbers. This undoubtly will give higher drag differential than the ideal case without separation. From these comparisons we may observe that the additional drag induced by the effective area due to lift on the equivalent body is close to the wave drag generated by lift in the drag rise region. At the upper end of the transonic range the differential drag of the equivalent bodies is higher than that generated by lift.

5.0 CONCLUDING REMARKS

The experimental study of the transonic equivalence rule with lift presented in Reference 1 has been extended to include a swept-back wing-body and the corresponding equivalent bodies of revoluation for lifting and non-lifting cases. The results of the analysis of the wave drag and drag rise in the transonic range are summarized as follows:

1. For zero lift drag the swept wing-body has the same drag rise characteristics as the delta wing-body with the same sweep-back parameter $\tilde{\lambda}$ up to Mach number about 0.97. At higher Mach number, the drag of the swept wing-body is higher than that of the delta wing-body.

2. The equivalent body for the swept wing-body at zero lift has much lower wave drag than the wing-body. The high wave drag of the wing-body is attributed to the shock formation along the span and the flow separation at the outer portion of the wing.

3. The drag rise due to lift is directly related to the square of the lift parameter $\tilde{\epsilon}\frac{\tilde{\alpha}}{\tilde{\tau}}$ for configurations with the same sweep-back parameter $\tilde{\lambda}$. For configurations with large difference in $\tilde{\lambda}$, the lift parameter is in the form of $\bar{C}_L{}^2/A$. When the flow over the wing is supersonic, the lift parameter $\tilde{\epsilon}\frac{\tilde{\alpha}}{\tilde{\tau}}$ should be used regardless of the value of $\tilde{\lambda}$. The planform shape has only small effect on the drag rise.

4. The additional drag induced by the effective area due to lift on the equivalent body agrees reasonably with the wave drag generated by lift on the wing-body.

From these results, we may conclude that the area rule for zero lift does not work well for swept-back wing-bodies with moderate aspect ratio as observed by other authors in area rule experiments[6,8]. The area rule due to lift as stated in (3) and (4) above, works reasonably well. It is therefore essental to include the additional effective area due to lift in the consideration of area rule for the design of transonic configurations.

6.0 REFERENCES

1. Chan, Y.Y. — *An Experimental Study of the Transonic Equivalence Rule with Lift.* NAE, Aeronautical Report LR-609, National Research Council Canada, March 1982.

2. Cheng, H.K. Hafez, M.M. — *Transonic Equivalance Rule: A Nonlinear Problem Involving Lift.* J. Fluid Mech., Vol. 72, Part 1, 1975, pp. 161-187.

3. Cheng, H.K. — *Lift Corrections to Transonic Equivalence Rule, Examples.* AIAA Journal, Vol. 15, No. 3, March 1977, pp. 366-373.

4. Relf, E.F. — *Note on the Drag of Thin Airfoils.* Perf. 1048, (Rept. 15582), British Aeronautical Research Council, January 1953.

5. Lock, R.C. Bridgewater, J. — *Theory of Aerodynamic Design for Swept-Winged Aircraft at Transonic and Supersonic Speeds.* IN "Progress in Aeronautical Sciences, Vol. 8." Ed. D. Küchemann, Pergamon Press, Toronto, 1967.

6. Whitcomb, R.T. — *A Study of the Zero-Lift Drag-Rise Characteristics of Wing-Body Combinations Near the Speed of Sound.* NACA Report 1273, 1956.

7. Gustavsson, A.L. Mattsson, R. — *Transonic Wing Tunnel Tests of the PT3 Model, A Supercritical Wing on a Simple Body.* Tech. Note AU-1134, Part 1, The Aeronautical Research Institute of Sweden, 1974.

8. Agrell, N. Mattsson, R. Nyberg, S.-E. — *Investigation of the Transonic Drag Characteristics for Non-slender Wing-Body Combinations and their Equivalent Axisymmetric Bodies at Zero Lift.* Proceedings of 11th Congress of the International Council of the Aeronautical Sciences, Vol. II, September 1978, pp. 292-304.

9. Küchemann, D. — *The Aerodynamic Design of Aircraft.* Pergamon Press, Toronto, Chapter 4, 1978.

10. Cheng, H.K. — *On Lifting-Line Theory in Unsteady Aerodynamics.* USCAE 133, Department of Aerospace Engineering, University of Southern California, January 1976.

11. Schmitt, V. Charpin, F. — *Pressure Distributions on the ONERA-M6-WING at Transonic Mach Number.* AGARD-AR-138, Experimental Data Base for Computer Program Assessment, May 1979.

12. Treadgold, D. Wilson, R.H. — *Some Aerodynamic Interference Effects that Influence the Transonic Performance of Combat Aircraft.* AGARD-CP-285, Subsonic/Transonic Configuration Aerodynamics, September 1980.

13. Schlichting, H. Truckenbrodt, E. — *Aerodynamics of the Airplane.* McGraw Hill, New York, 1979.

14. Frick, C.W.
The Experimental Aerodynamics of Wings at Transonic and Supersonic Speeds.
IN "Aerodynamic Components of Aircraft at High Speed." Ed. A.F. Donovan and H.R. Lawrence, Princeton University Press, Princeton, New Jersey, 1957.

15. Jones, R.T.
Cohen, D.
Aerodynamics of Wings at High Speeds.
IN "Aerodynamic Components of Aircraft at High Speed." Ed. A.F. Donovan and H.R. Lawrence, Princeton University Press, Princeton, New Jersey, 1957.

16. Allis, A.E. et al
Experimental Investigation of Parametric Models in Support of a NASA Advanced Transport Technology Program.
Vol. 1, Data Summary, NASA CR-112130, October 1972.

17. Spreiter, J.R.
On the Range of Application of the Transonic Area Rule.
NACA TN 3673, 1956.

TABLE 1

DIMENSIONS AND PARAMETERS OF THE SWEPT WING-BODY MODEL WBS

Body length	ℓ = 17.5 in. (444.5 mm)
Body radius	r = 0.875 in. (22.23 mm)
Semi-span	b = 7.56 in. (192.0 mm)
Mean aerodynamic chord	c_m = 2.98 in. (75.7 mm)
Root chord	C_r = 4.2857 in. (108.8 mm)
Taper chord	λ = 0.4
Leading edge swept angle	Λ = 38.435°
Aspect ratio	A = 5.04
Wing thickness	t/c = 0.057
Wing swept parameter	$\tilde{\lambda}$ = 0.4320
Thickness parameter	$\tilde{\tau}$ = 0.0275

TABLE 2

SOME GEOMETRIC PARAMETERS OF THE SWEPT WING AND THE DELTA WING MODELS

	WB1	WB2	WBS
c_0 (in.)	6.000	6.000	7.715
b (in.)	4.044	7.286	7.560
S_w (in.^{2})	25.155	45.278	45.106
S_c (in.^{2})	3.647	3.647	3.641
c_0/ℓ	0.343	0.343	0.441
A	2.600	4.690	5.068
$\tilde{\lambda}$	0.231	0.416	0.432
$\tilde{\tau}$	0.0497	0.0276	0.0275
$\tilde{\tau}\tilde{\lambda}$	0.0115	0.0115	0.0119

TABLE 3

AERODYNAMIC COEFFICIENTS OF SWEPT WING-BODY MODEL WBS

MACH NO.=0.799 M=31
RE/FT(M)=7.79

ALPHAB	CLB	CD
-3.0844	-0.2378	0.0171
-2.7762	-0.2182	0.0157
-2.4653	-0.1990	0.0147
-2.2431	-0.1739	0.0139
-1.9400	-0.1502	0.0131
-1.6465	-0.1295	0.0124
-1.3658	-0.1034	0.0119
-1.0668	-0.0767	0.0116
-0.7880	-0.0614	0.0113
-0.5167	-0.0441	0.0111
-0.2085	-0.0130	0.0111
0.0750	0.0058	0.0111
0.3352	0.0185	0.0113
0.6461	0.0481	0.0113
0.9163	0.0681	0.0116
1.2298	0.1014	0.0117
1.5098	0.1182	0.0123
1.7883	0.1428	0.0130
2.0789	0.1647	0.0139
2.3840	0.1956	0.0149
2.6639	0.2186	0.0162
2.9599	0.2449	0.0176
3.2312	0.2627	0.0191
3.5179	0.2838	0.0210
3.7939	0.3006	0.0228
4.0823	0.3227	0.0248
4.3676	0.3483	0.0275
4.6769	0.3830	0.0306
4.9613	0.4056	0.0336
5.2585	0.4275	0.0369
5.4968	0.4477	0.0400

MACH NO.=0.847 M=31
RE/FT(M)=7.76

ALPHAB	CLB	CD
-2.9678	-0.2309	0.0170
-2.6704	-0.2079	0.0158
-2.3489	-0.1823	0.0147
-2.1368	-0.1692	0.0140
-1.8309	-0.1461	0.0132
-1.5259	-0.1248	0.0126
-1.2446	-0.0993	0.0120
-0.9469	-0.0715	0.0116
-0.6628	-0.0508	0.0113
-0.3618	-0.0231	0.0112
-0.0643	0.0050	0.0111
0.2016	0.0153	0.0111
0.4934	0.0389	0.0112
0.7783	0.0625	0.0113
1.0520	0.0791	0.0117
1.3390	0.0991	0.0121
1.6354	0.1268	0.0127
1.9409	0.1591	0.0134
2.2307	0.1780	0.0143
2.5354	0.2153	0.0155
2.8222	0.2370	0.0168
3.1099	0.2636	0.0184
3.4094	0.2912	0.0202
3.7043	0.3158	0.0223
4.0002	0.3453	0.0246
4.2979	0.3745	0.0273
4.5702	0.3893	0.0298
4.8757	0.4225	0.0334
5.1695	0.4503	0.0371
5.4499	0.4715	0.0407
5.7088	0.5029	0.0456

MACH NO.=0.894 M=31
RE/FT(M)=7.74

ALPHAB	CLB	CD
-3.0891	-0.2719	0.0186
-2.7755	-0.2362	0.0167
-2.4570	-0.2013	0.0152
-2.2271	-0.1812	0.0143
-1.9039	-0.1517	0.0134
-1.6057	-0.1282	0.0128
-1.3318	-0.1147	0.0122
-1.0573	-0.0937	0.0118
-0.7598	-0.0688	0.0114
-0.4460	-0.0361	0.0112
-0.1449	-0.0075	0.0111
0.1384	0.0115	0.0113
0.4064	0.0277	0.0113
0.7210	0.0590	0.0116
1.0060	0.0809	0.0119
1.3039	0.1104	0.0122
1.6029	0.1391	0.0128
1.8920	0.1584	0.0137
2.2026	0.1921	0.0149
2.5132	0.2311	0.0163
2.8197	0.2623	0.0181
3.1044	0.2894	0.0199
3.4207	0.3267	0.0227
3.7393	0.3685	0.0260
4.0430	0.3990	0.0293
4.3227	0.4213	0.0326
4.6165	0.4486	0.0366
4.9165	0.4769	0.0411
5.2265	0.5160	0.0469
5.5150	0.5368	0.0517
5.7660	0.5628	0.0568

MACH NO.=0.912 M=31
RE/FT(M)=7.70

ALPHAB	CLB	CD
-3.1551	-0.2959	0.0208
-2.8119	-0.2554	0.0182
-2.4990	-0.2243	0.0163
-2.2508	-0.1986	0.0152
-1.9402	-0.1699	0.0141
-1.6108	-0.1378	0.0131
-1.3301	-0.1116	0.0126
-1.0574	-0.0899	0.0120
-0.7506	-0.0637	0.0117
-0.4627	-0.0411	0.0115
-0.1567	-0.0148	0.0114
0.1318	0.0054	0.0114
0.4357	0.0396	0.0114
0.7206	0.0618	0.0116
1.0279	0.0918	0.0119
1.3065	0.1121	0.0125
1.5985	0.1381	0.0133
1.8953	0.1626	0.0142
2.2104	0.2022	0.0154
2.5230	0.2339	0.0171
2.8464	0.2791	0.0193
3.1756	0.3069	0.0217
3.4293	0.3353	0.0244
3.7356	0.3687	0.0278
4.0331	0.4034	0.0314
4.3468	0.4403	0.0359
4.6533	0.4758	0.0411
4.9552	0.5063	0.0461
5.2515	0.5361	0.0511
5.5468	0.5617	0.0564
5.8009	0.5745	0.0604

TABLE 3

AERODYNAMIC COEFFICIENTS OF SWEPT WING-BODY MODEL WBS (Cont'd)

MACH NO.=0.931 M=31
RE/FT(M)=7.68

ALPHAB	CLB	CD
-3.0465	-0.2895	0.0226
-2.7221	-0.2493	0.0198
-2.3914	-0.2130	0.0176
-2.1697	-0.1952	0.0165
-1.8557	-0.1703	0.0151
-1.5415	-0.1403	0.0140
-1.2720	-0.1175	0.0133
-0.9827	-0.0975	0.0126
-0.6490	-0.0571	0.0120
-0.3526	-0.0288	0.0119
-0.0920	-0.0182	0.0118
0.2254	0.0203	0.0118
0.5235	0.0480	0.0120
0.8216	0.0777	0.0124
1.1157	0.1050	0.0128
1.3975	0.1266	0.0136
1.7203	0.1647	0.0148
2.0267	0.1976	0.0160
2.3314	0.2294	0.0178
2.6285	0.2597	0.0199
2.9398	0.2944	0.0223
3.2402	0.3287	0.0252
3.5350	0.3611	0.0285
3.8440	0.3973	0.0323
4.1334	0.4223	0.0361
4.4366	0.4532	0.0405
4.7507	0.4903	0.0458
5.0416	0.5083	0.0500
5.2916	0.5186	0.0532
5.6262	0.5606	0.0602
5.8384	0.5751	0.0636

MACH NO.=0.948 M=31
RE/FT(M)=7.74

ALPHAB	CLB	CD
-3.1560	-0.3018	0.0262
-2.8580	-0.2718	0.0236
-2.5274	-0.2344	0.0210
-2.2882	-0.2052	0.0194
-1.9651	-0.1789	0.0178
-1.6644	-0.1524	0.0165
-1.3846	-0.1243	0.0154
-1.0989	-0.1065	0.0146
-0.7821	-0.0735	0.0139
-0.5012	-0.0524	0.0135
-0.1972	-0.0219	0.0133
0.0966	0.0075	0.0133
0.3921	0.0347	0.0135
0.7013	0.0666	0.0138
1.0024	0.0954	0.0144
1.2867	0.1196	0.0152
1.5862	0.1511	0.0164
1.8948	0.1826	0.0177
2.1783	0.2038	0.0193
2.4930	0.2446	0.0216
2.7995	0.2750	0.0241
3.0918	0.3031	0.0267
3.4044	0.3397	0.0301
3.7002	0.3716	0.0339
3.9802	0.3898	0.0369
4.2935	0.4280	0.0416
4.5903	0.4540	0.0458
4.8651	0.4755	0.0500
5.1662	0.5011	0.0548
5.4475	0.5231	0.0593
5.7010	0.5479	0.0639

MACH NO.=0.965 M=31
RE/FT(M)=7.73

ALPHAB	CLB	CD
-3.1438	-0.2848	0.0295
-2.8377	-0.2519	0.0269
-2.5022	-0.2165	0.0244
-2.2940	-0.1972	0.0230
-1.9594	-0.1641	0.0212
-1.6764	-0.1415	0.0199
-1.3887	-0.1171	0.0190
-1.0860	-0.0878	0.0180
-0.7750	-0.0607	0.0172
-0.4928	-0.0386	0.0168
-0.2091	-0.0194	0.0167
0.0811	0.0054	0.0166
0.3596	0.0236	0.0169
0.6739	0.0559	0.0173
0.9388	0.0709	0.0178
1.2489	0.1058	0.0185
1.5536	0.1388	0.0197
1.8486	0.1595	0.0210
2.1262	0.1814	0.0223
2.4529	0.2251	0.0245
2.7589	0.2591	0.0270
3.0636	0.2978	0.0298
3.3559	0.3184	0.0325
3.6416	0.3479	0.0356
3.9430	0.3759	0.0394
4.2649	0.4139	0.0439
4.5587	0.4464	0.0483
4.8463	0.4710	0.0524
5.1487	0.4968	0.0570
5.4217	0.5120	0.0608
5.6794	0.5329	0.0651

MACH NO.=0.979 M=31
RE/FT(M)=7.66

ALPHAB	CLB	CD
-2.9850	-0.2585	0.0324
-2.6669	-0.2264	0.0299
-2.3475	-0.1946	0.0278
-2.1295	-0.1798	0.0268
-1.8015	-0.1492	0.0250
-1.4862	-0.1192	0.0238
-1.2250	-0.1061	0.0231
-0.9394	-0.0779	0.0223
-0.6176	-0.0435	0.0216
-0.3461	-0.0274	0.0214
-0.0480	-0.0087	0.0214
0.2375	0.0135	0.0216
0.5102	0.0316	0.0218
0.8293	0.0654	0.0223
1.1127	0.0896	0.0229
1.4417	0.1301	0.0239
1.7159	0.1502	0.0248
2.0151	0.1737	0.0263
2.3087	0.2043	0.0290
2.5997	0.2305	0.0297
2.8835	0.2513	0.0314
3.2139	0.2980	0.0347
3.5212	0.3340	0.0376
3.8129	0.3591	0.0407
4.1041	0.3890	0.0441
4.3955	0.4141	0.0477
4.6883	0.4446	0.0519
4.9948	0.4717	0.0560
5.2837	0.4969	0.0604
5.5752	0.5208	0.0650
5.8048	0.5410	0.0687

TABLE 3
AERODYNAMIC COEFFICIENTS OF SWEPT WING-BODY MODEL WBS (Cont'd)

MACH NO.=0.997 M=31
RE/FT(M)=7.67

ALPHAB	CLB	CD
-2.9838	-0.2623	0.0353
-2.6726	-0.2332	0.0331
-2.3785	-0.2079	0.0313
-2.1337	-0.1791	0.0299
-1.7981	-0.1462	0.0283
-1.4978	-0.1232	0.0273
-1.2362	-0.1012	0.0266
-0.9382	-0.0784	0.0258
-0.6376	-0.0514	0.0253
-0.3496	-0.0276	0.0250
-0.0612	-0.0059	0.0248
0.2422	0.0196	0.0250
0.5116	0.0374	0.0251
0.8203	0.0696	0.0255
1.0961	0.0886	0.0262
1.3980	0.1138	0.0272
1.7028	0.1435	0.0281
1.9766	0.1632	0.0292
2.2914	0.1998	0.0310
2.5812	0.2247	0.0326
2.8715	0.2513	0.0345
3.1954	0.2893	0.0372
3.4900	0.3208	0.0401
3.7757	0.3454	0.0428
4.0868	0.3797	0.0464
4.3833	0.4111	0.0501
4.6677	0.4289	0.0533
4.9435	0.4484	0.0565
5.2671	0.4918	0.0622
5.5528	0.5126	0.0663
5.8045	0.5359	0.0704

MACH NO.=1.016 M=31
RE/FT(M)=7.67

ALPHAB	CLB	CD
-2.9782	-0.2628	0.0374
-2.6180	-0.2277	0.0349
-2.2971	-0.1952	0.0330
-2.0618	-0.1732	0.0318
-1.7524	-0.1438	0.0305
-1.4551	-0.1192	0.0295
-1.1611	-0.0929	0.0287
-0.8657	-0.0713	0.0280
-0.5725	-0.0461	0.0276
-0.2956	-0.0291	0.0274
0.0072	-0.0047	0.0272
0.3013	0.0240	0.0273
0.5768	0.0452	0.0276
0.8726	0.0668	0.0280
1.1755	0.0884	0.0288
1.4686	0.1276	0.0298
1.7745	0.1513	0.0309
2.0693	0.1833	0.0322
2.3940	0.2197	0.0340
2.6459	0.2320	0.0354
2.9298	0.2570	0.0374
3.2530	0.2940	0.0400
3.5489	0.3254	0.0429
3.8512	0.3547	0.0457
4.1514	0.3875	0.0492
4.4628	0.4223	0.0533
4.7586	0.4497	0.0571
5.0261	0.4665	0.0602
5.3346	0.4974	0.0650
5.6338	0.5275	0.0700
5.8740	0.5506	0.0740

MACH NO.=1.036 M=31
RE/FT(M)=7.67

ALPHAB	CLB	CD
-3.0404	-0.2596	0.0389
-2.7351	-0.2313	0.0367
-2.4168	-0.2021	0.0349
-2.1671	-0.1804	0.0336
-1.8651	-0.1552	0.0324
-1.5732	-0.1333	0.0313
-1.2807	-0.1051	0.0303
-0.9848	-0.0810	0.0296
-0.6938	-0.0565	0.0291
-0.4043	-0.0306	0.0287
-0.1215	-0.0119	0.0286
0.1544	0.0048	0.0285
0.4662	0.0358	0.0288
0.7757	0.0688	0.0292
1.0475	0.0898	0.0297
1.3508	0.1155	0.0306
1.6289	0.1337	0.0315
1.9390	0.1650	0.0330
2.2229	0.1873	0.0342
2.5179	0.2172	0.0359
2.8142	0.2427	0.0379
3.1440	0.2831	0.0405
3.4257	0.3070	0.0427
3.7161	0.3332	0.0456
3.9910	0.3499	0.0481
4.3112	0.3852	0.0519
4.5900	0.4060	0.0552
4.8924	0.4385	0.0593
5.2105	0.4774	0.0646
5.4817	0.4916	0.0680
5.7337	0.5060	0.0713

MACH NO.=1.054 M=31
RE/FT(M)=7.64

ALPHAB	CLB	CD
-2.9906	-0.2574	0.0378
-2.6937	-0.2322	0.0358
-2.3774	-0.2022	0.0338
-2.1413	-0.1771	0.0325
-1.8297	-0.1507	0.0310
-1.5044	-0.1221	0.0299
-1.2482	-0.1074	0.0292
-0.9537	-0.0792	0.0284
-0.6660	-0.0585	0.0278
-0.3717	-0.0315	0.0274
-0.0697	-0.0025	0.0272
0.2360	0.0247	0.0273
0.5003	0.0399	0.0275
0.7959	0.0629	0.0280
1.0866	0.0912	0.0287
1.3664	0.1051	0.0294
1.6912	0.1478	0.0307
1.9757	0.1716	0.0319
2.2726	0.1984	0.0334
2.5834	0.2332	0.0355
2.8701	0.2538	0.0374
3.1553	0.2732	0.0394
3.4445	0.3007	0.0418
3.7581	0.3335	0.0450
4.0597	0.3684	0.0486
4.3585	0.3977	0.0521
4.6629	0.4257	0.0558
4.9366	0.4426	0.0593
5.2327	0.4707	0.0635
5.5347	0.4968	0.0680
5.7720	0.5121	0.0713

TABLE 3

AERODYNAMIC COEFFICIENTS OF SWEPT WING-BODY MODEL WBS (Cont'd)

MACH NO.=1.084 M=31
RE/FT(M)=7.75

ALPHAB	CLB	CD
-3.0082	-0.2647	0.0389
-2.6773	-0.2274	0.0361
-2.3528	-0.1994	0.0341
-2.1385	-0.1814	0.0330
-1.8279	-0.1585	0.0316
-1.5276	-0.1337	0.0305
-1.2390	-0.1045	0.0295
-0.9360	-0.0766	0.0286
-0.6313	-0.0495	0.0280
-0.3534	-0.0280	0.0277
-0.0669	-0.0068	0.0275
0.2352	0.0218	0.0276
0.5278	0.0450	0.0278
0.8090	0.0608	0.0283
1.1074	0.0939	0.0290
1.4029	0.1178	0.0299
1.7081	0.1506	0.0313
1.9934	0.1692	0.0325
2.2818	0.1905	0.0339
2.5541	0.2082	0.0354
2.8736	0.2467	0.0377
3.1702	0.2707	0.0399
3.4680	0.2980	0.0425
3.7575	0.3261	0.0453
4.0356	0.3450	0.0478
4.3513	0.3760	0.0514
4.6417	0.4049	0.0551
4.9318	0.4281	0.0588
5.2326	0.4564	0.0630
5.5291	0.4846	0.0676
5.7721	0.5034	0.0710

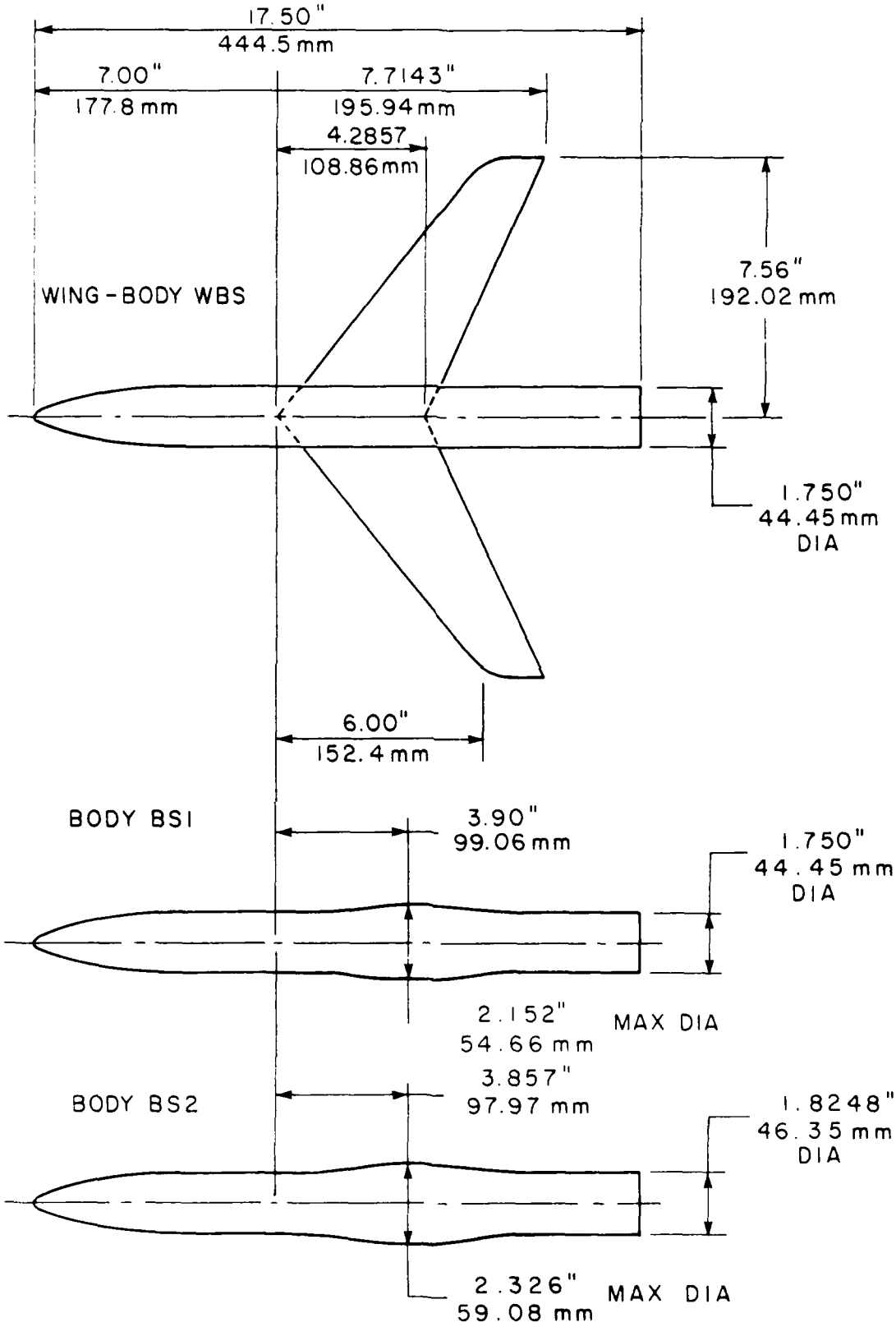

FIG. 1: THE SWEPT WING-BODY MODEL AND ITS EQUIVALENT BODIES

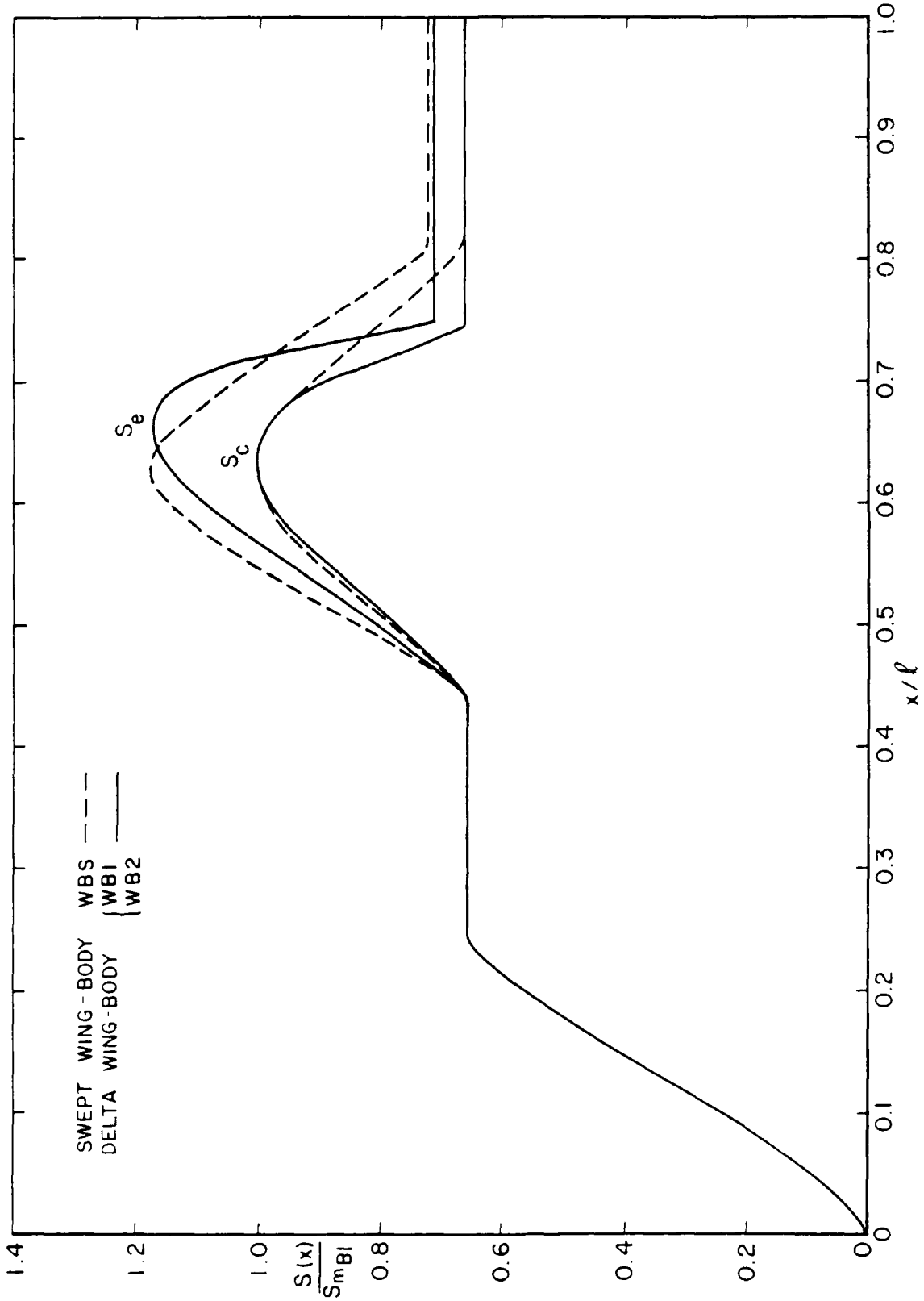

FIG. 2: CROSS-SECTIONAL AREA DISTRIBUTIONS OF THE MODELS WITH AND WITHOUT EFFECTIVE AREA DUE TO LIFT

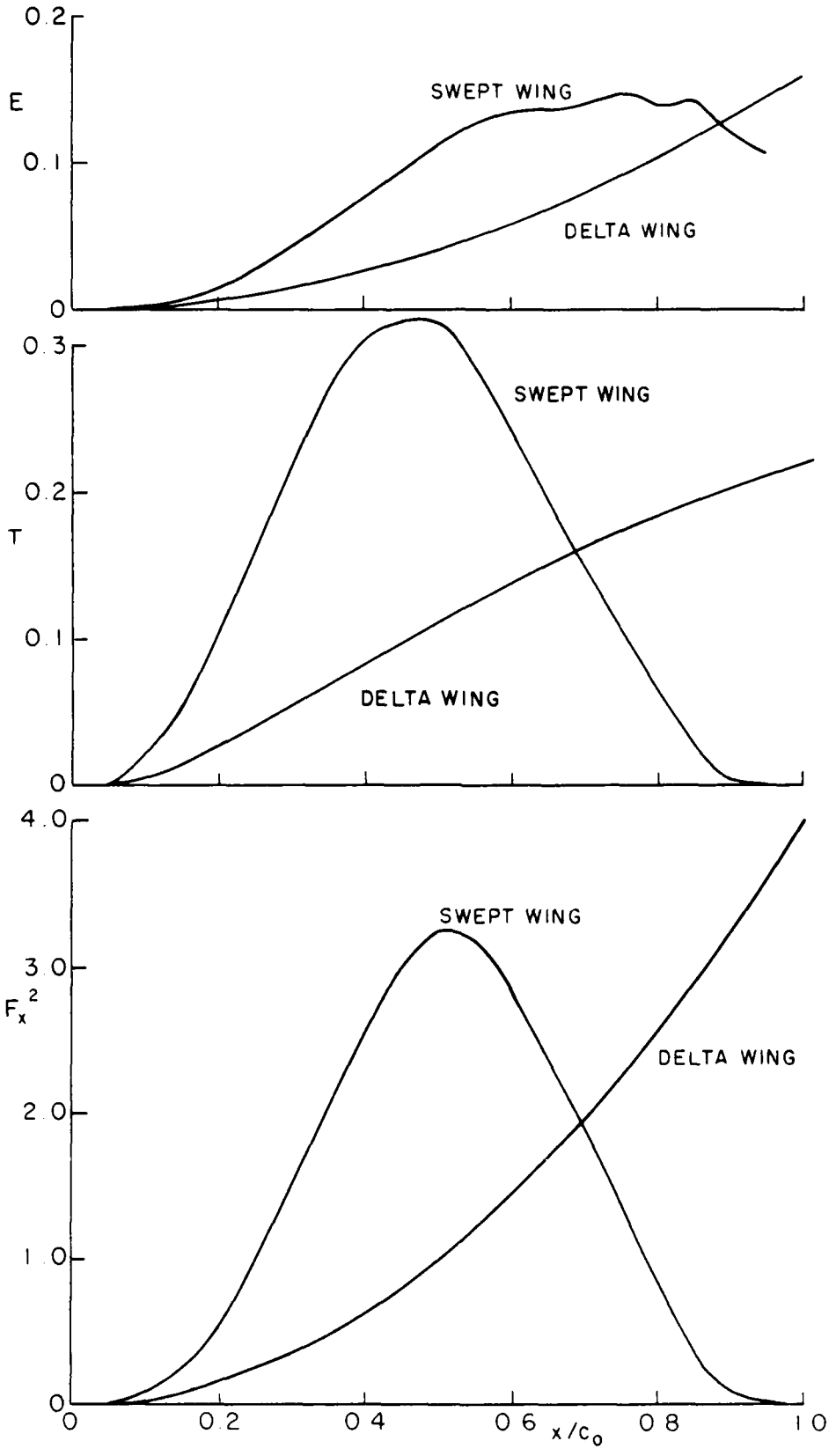

FIG. 3: FUNCTIONS DUE TO LIFT, E(x), T(x) AND F_x^2 FOR SWEPT-BACK AND DELTA PLANFORMS

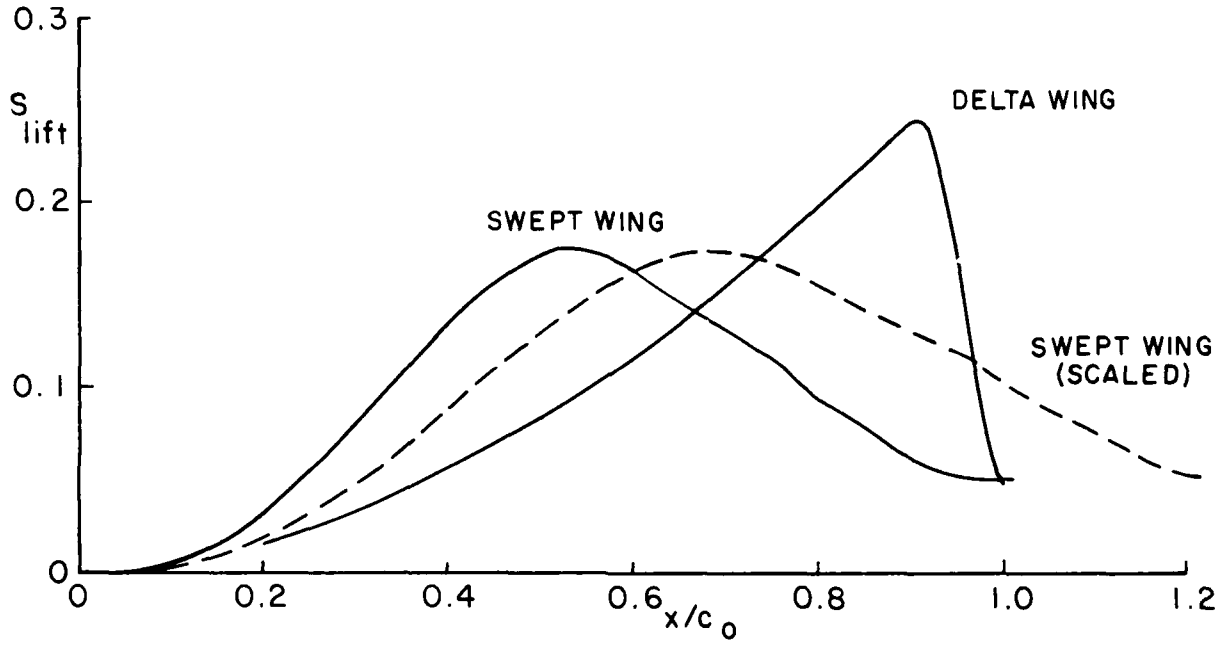

FIG. 4: DISTRIBUTIONS OF EFFECTIVE AREA DUE TO LIFT FOR SWEPT-BACK AND DELTA PLANFORMS AT THE DESIGN LIFT CONDITION

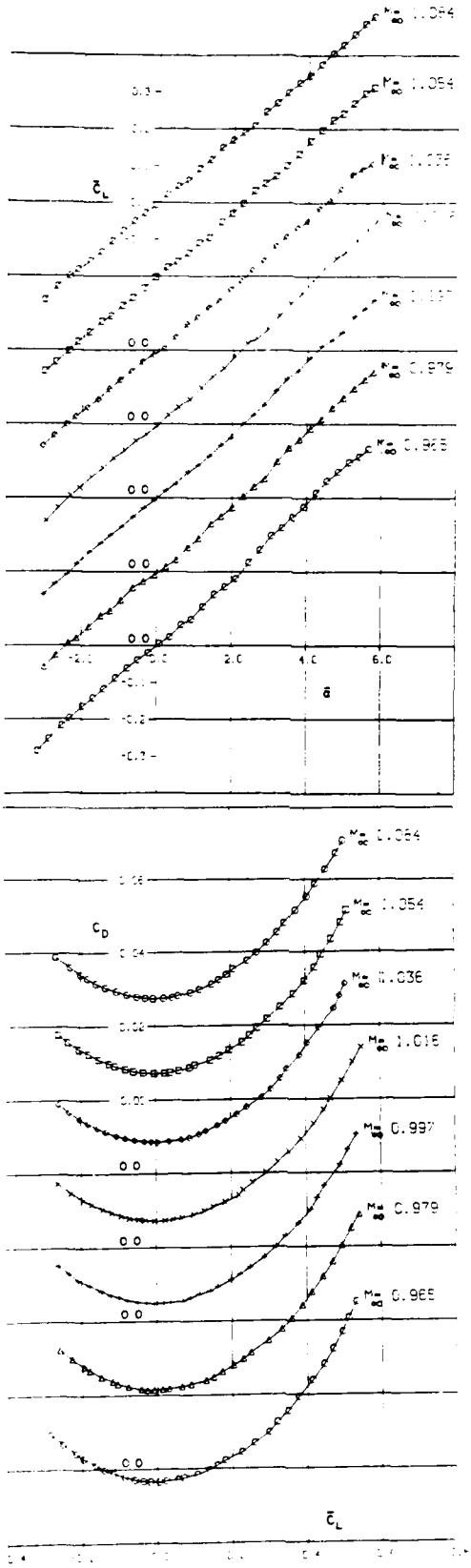

FIG. 5: VARIATIONS OF $\bar{C}_L$ WITH $\bar{\alpha}$ AND C_D WITH $\bar{C}_L$ FOR SWEPT WING-BODY MODEL WBS AT DIFFERENT MACH NUMBERS

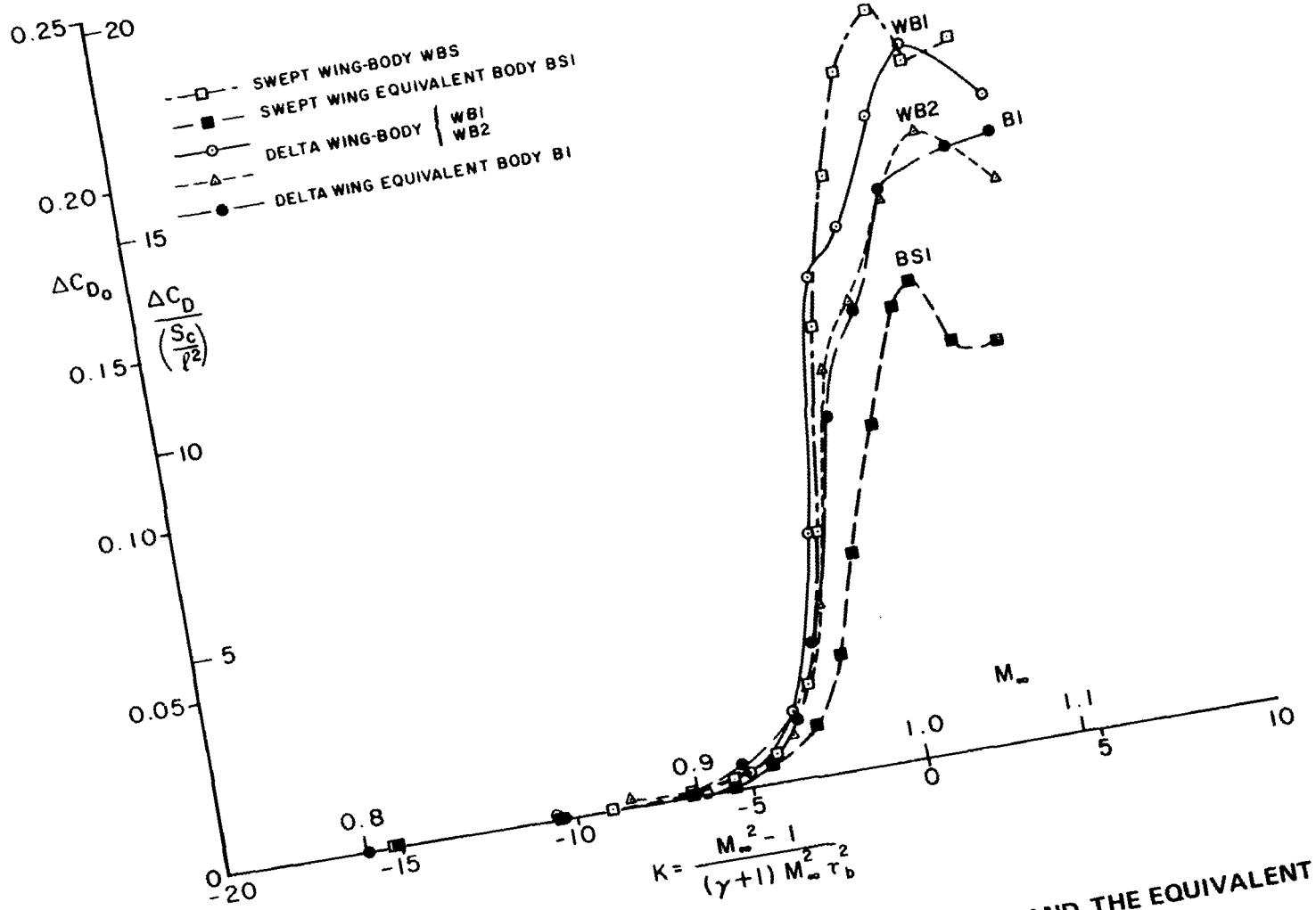

FIG. 6: ZERO LIFT DRAG RISE FOR THE SWEPT WING-BODY WBS AND THE EQUIVALENT BODY BS1

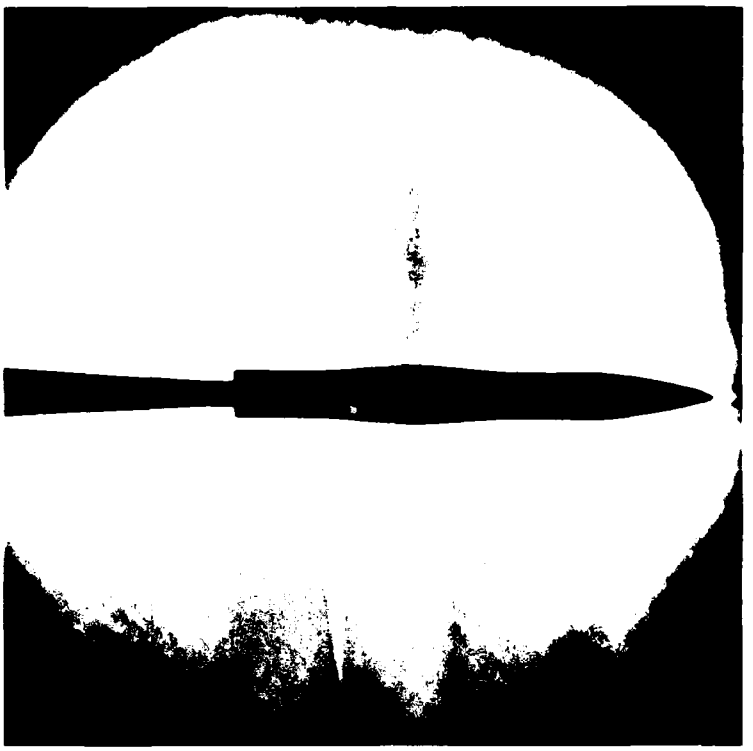

EQUIVALENT BODY BSI, $\alpha = -0.05°$

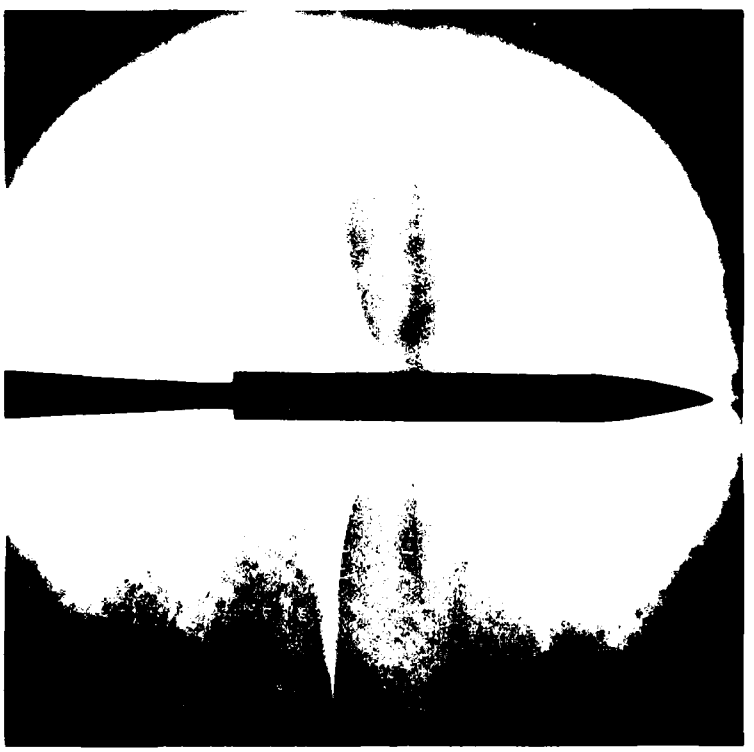

WING-BODY WBS, $\alpha = 0.01°$

FIG. 7: SCHLIEREN FLOW VISUALIZATION FOR WING-BODY WBS AND EQUIVALENT BODY BS1 AT ZERO ANGLE OF ATTACK (NOMINAL), $M_\infty = 0.98$

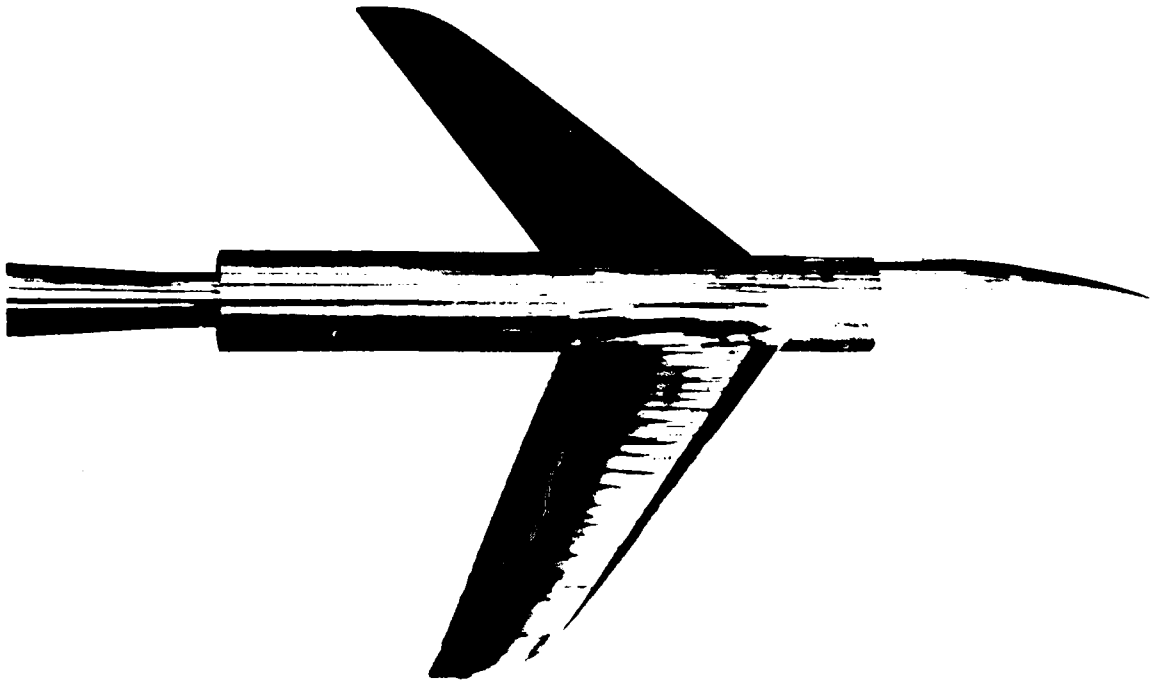

WING-BODY W1BS

EQUIVALENT BODY BS1

FIG. 8: SURFACE FLOW VISUALIZATION FOR WING-BODY WBS AND EQUIVALENT BODY BS1 AT ZERO ANGLE OF ATTACK, M_∞ = 0.98

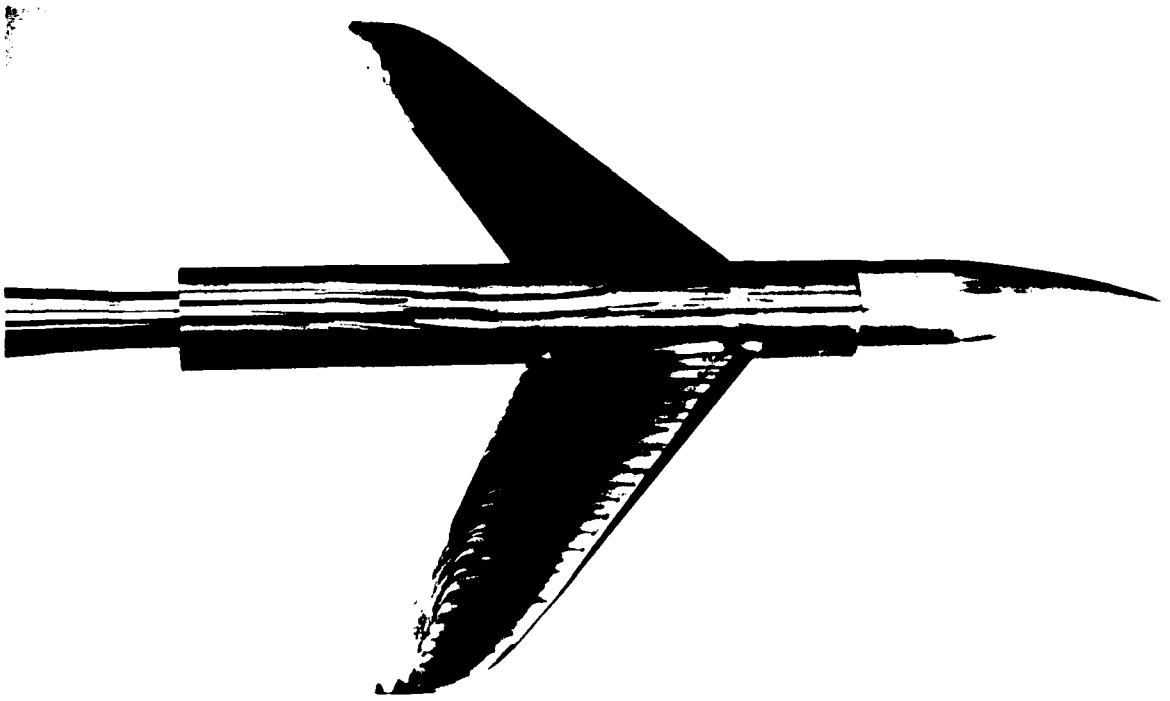

α = 2.94°

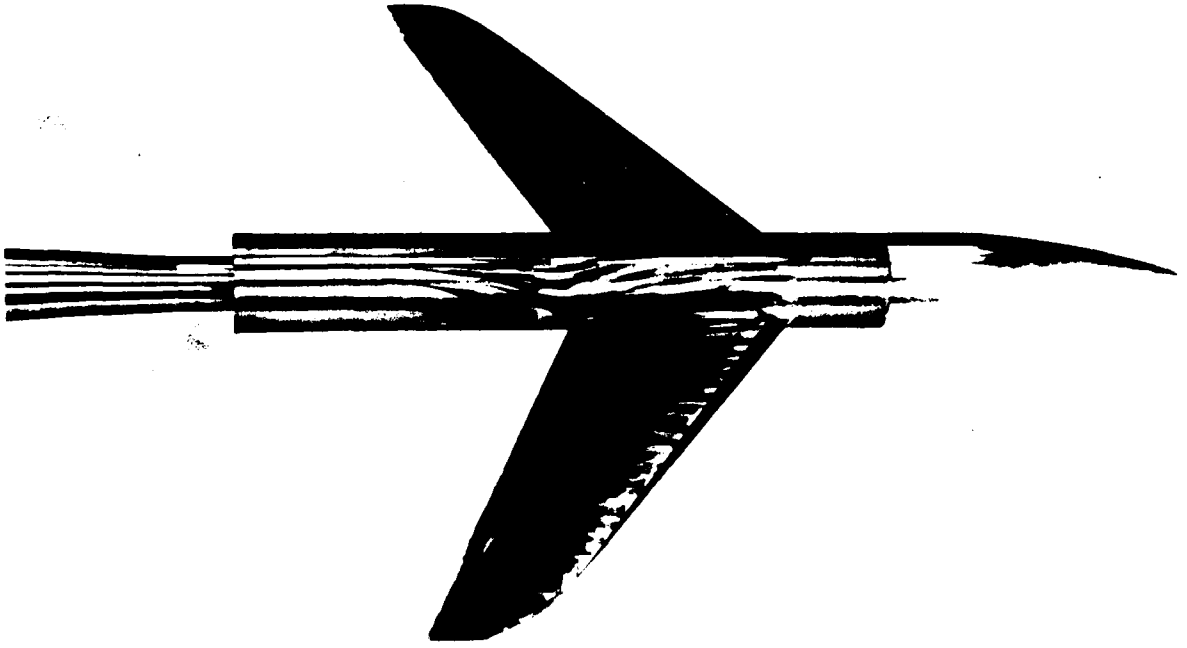

α = 5.51°

FIG. 9: SURFACE FLOW VISUALIZATION FOR WING-BODY MODEL WBS AT ANGLES OF ATTACK, M_∞ = 0.98

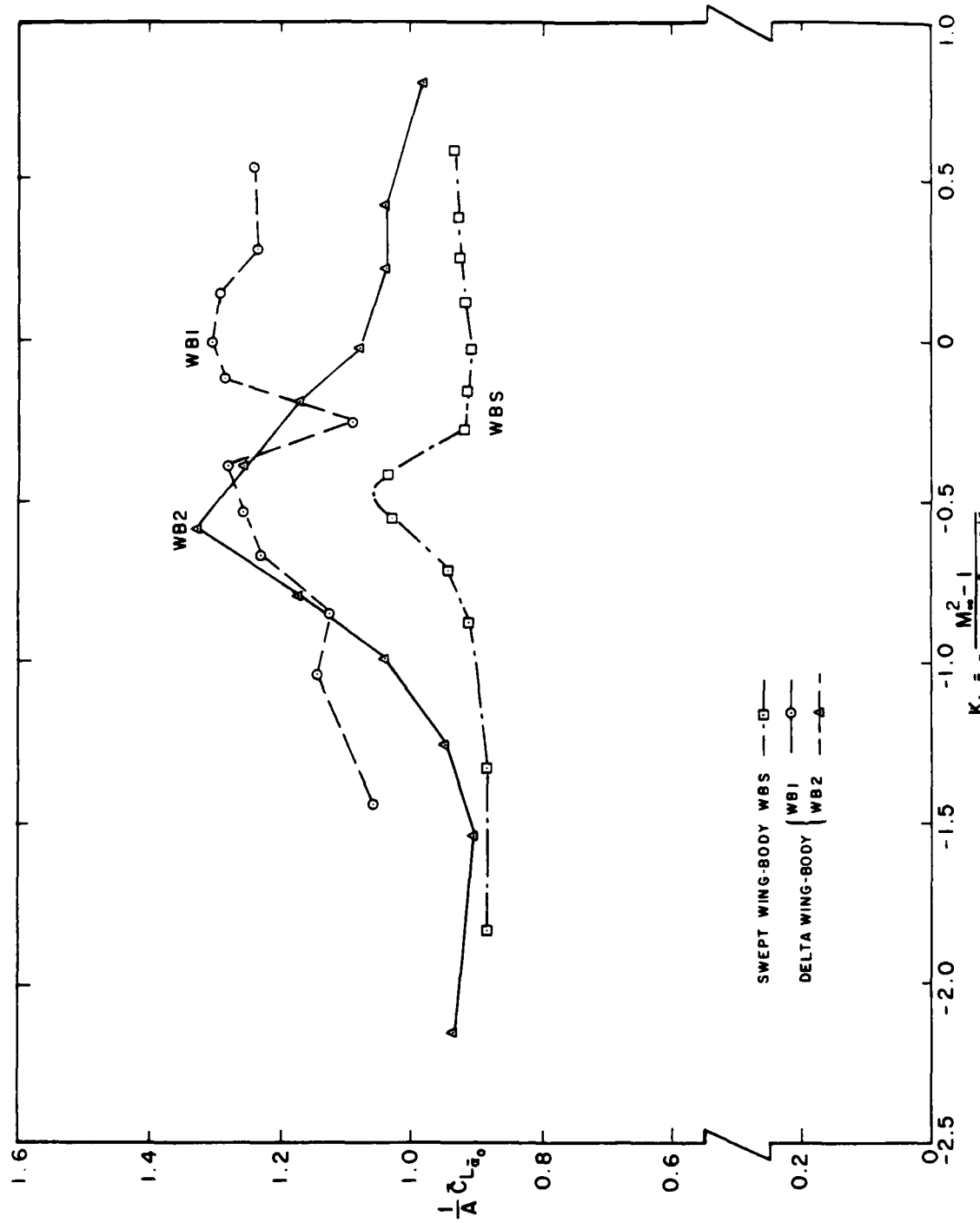

FIG. 10: VARIATIONS OF LIFT CURVE SLOPE AT ZERO LIFT WITH TRANSONIC SIMILARITY PARAMETER BASED ON THE WING THICKNESS TO CHORD RATIO FOR SWEPT WING AND DELTA WING MODELS

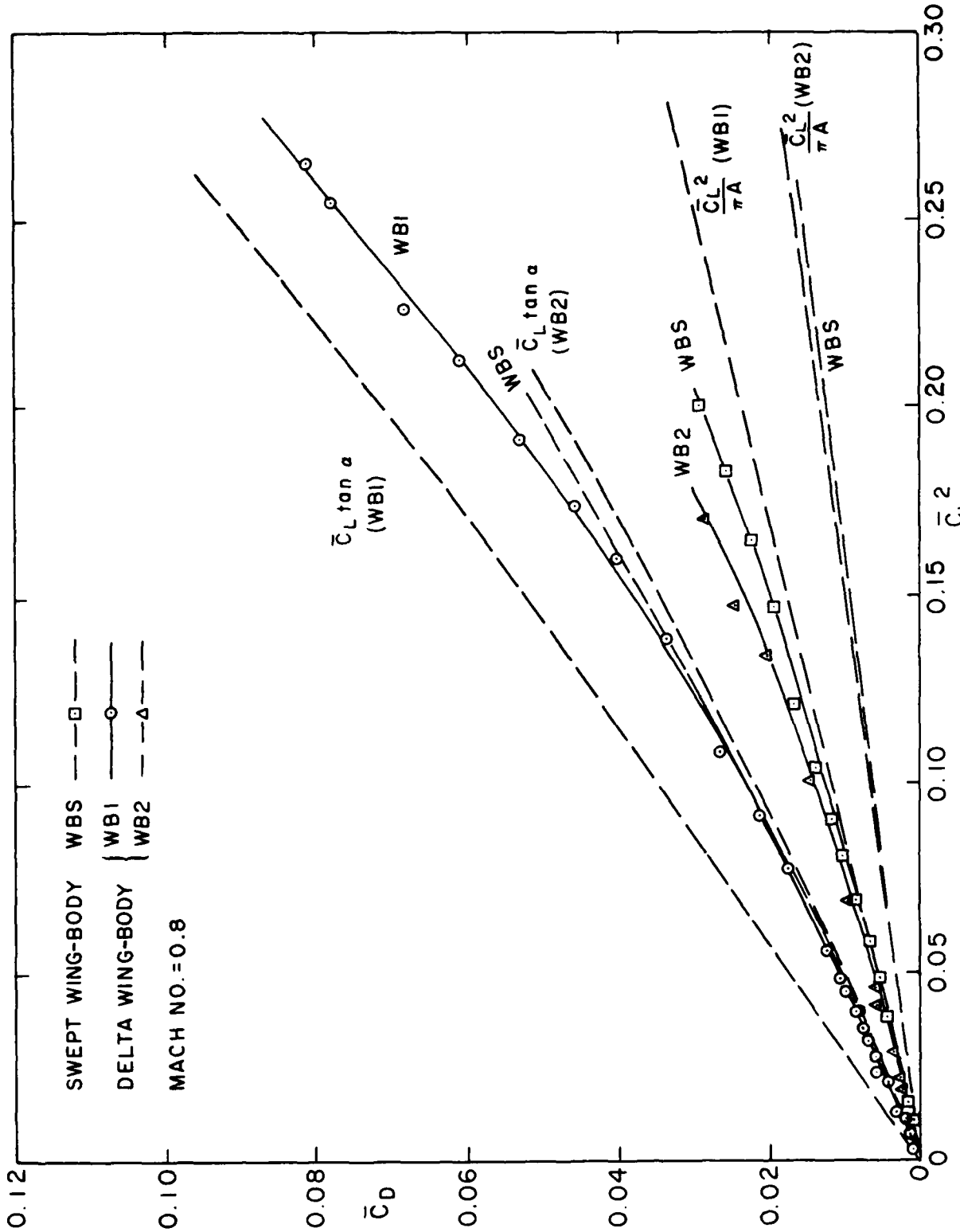

FIG. 11: VARIATIONS OF $\bar{C}_D$ WITH $\bar{C}_L^2$ FOR SWEPT WING AND DELTA WING MODELS AT MACH NUMBER 0.8

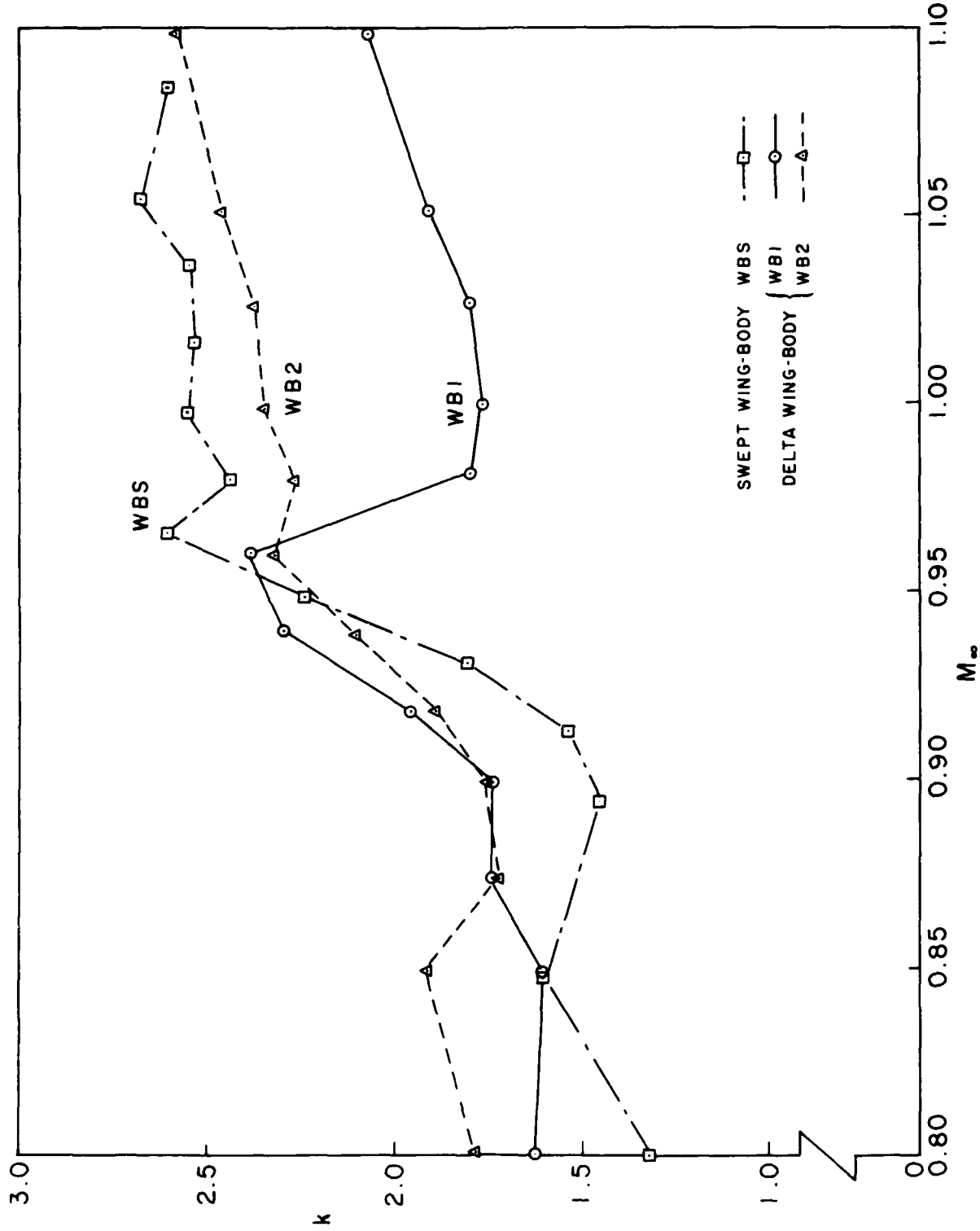

FIG. 12: VARIATIONS OF DRAG FACTOR k WITH MACH NUMBER FOR SWEPT WING AND DELTA WING MODELS

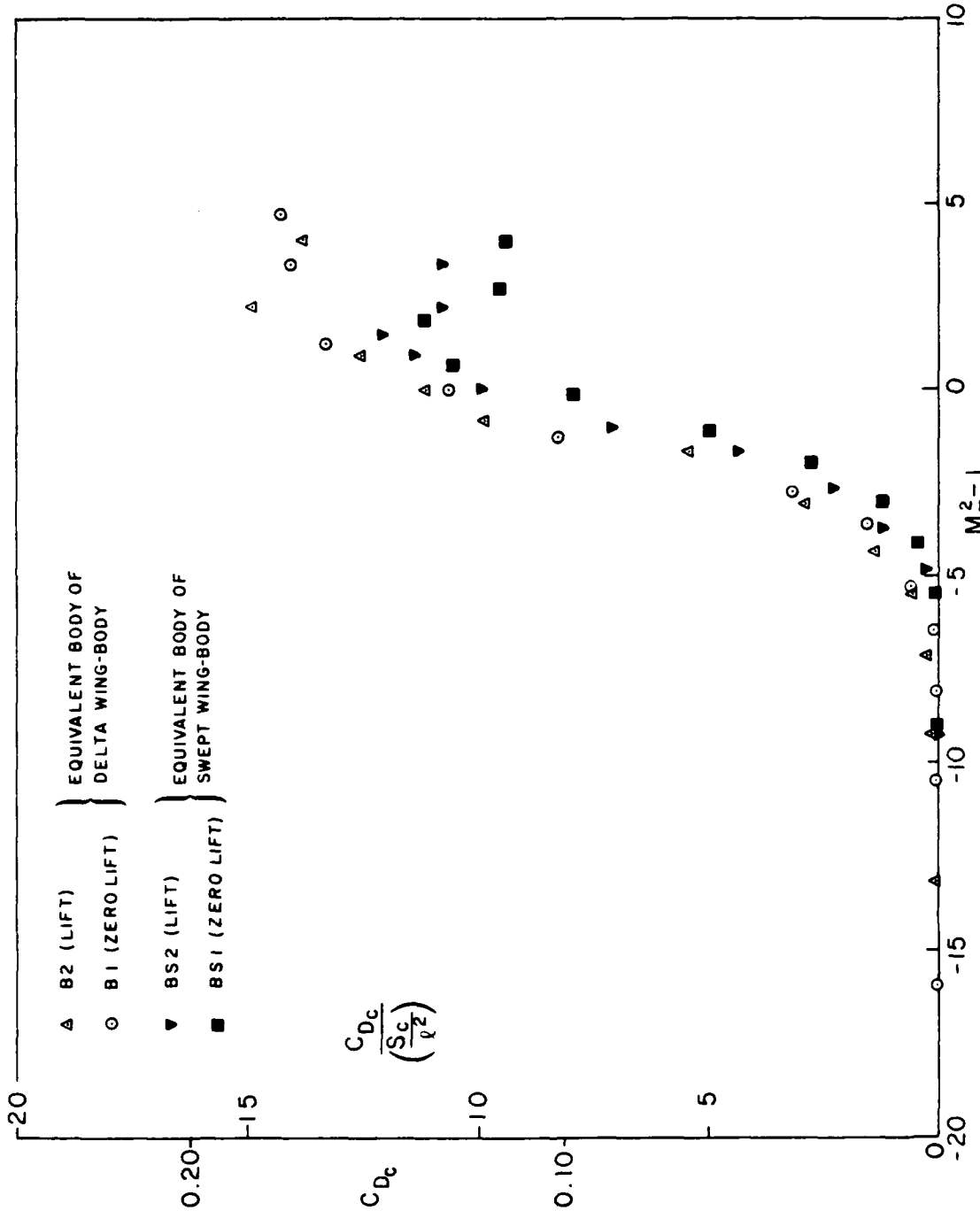

FIG. 13: DRAG-RISE FOR THE EQUIVALENT BODIES BS1, BS2 FOR THE SWEPT WING CASE AND B1, B2 FOR THE DELTA WING CASE

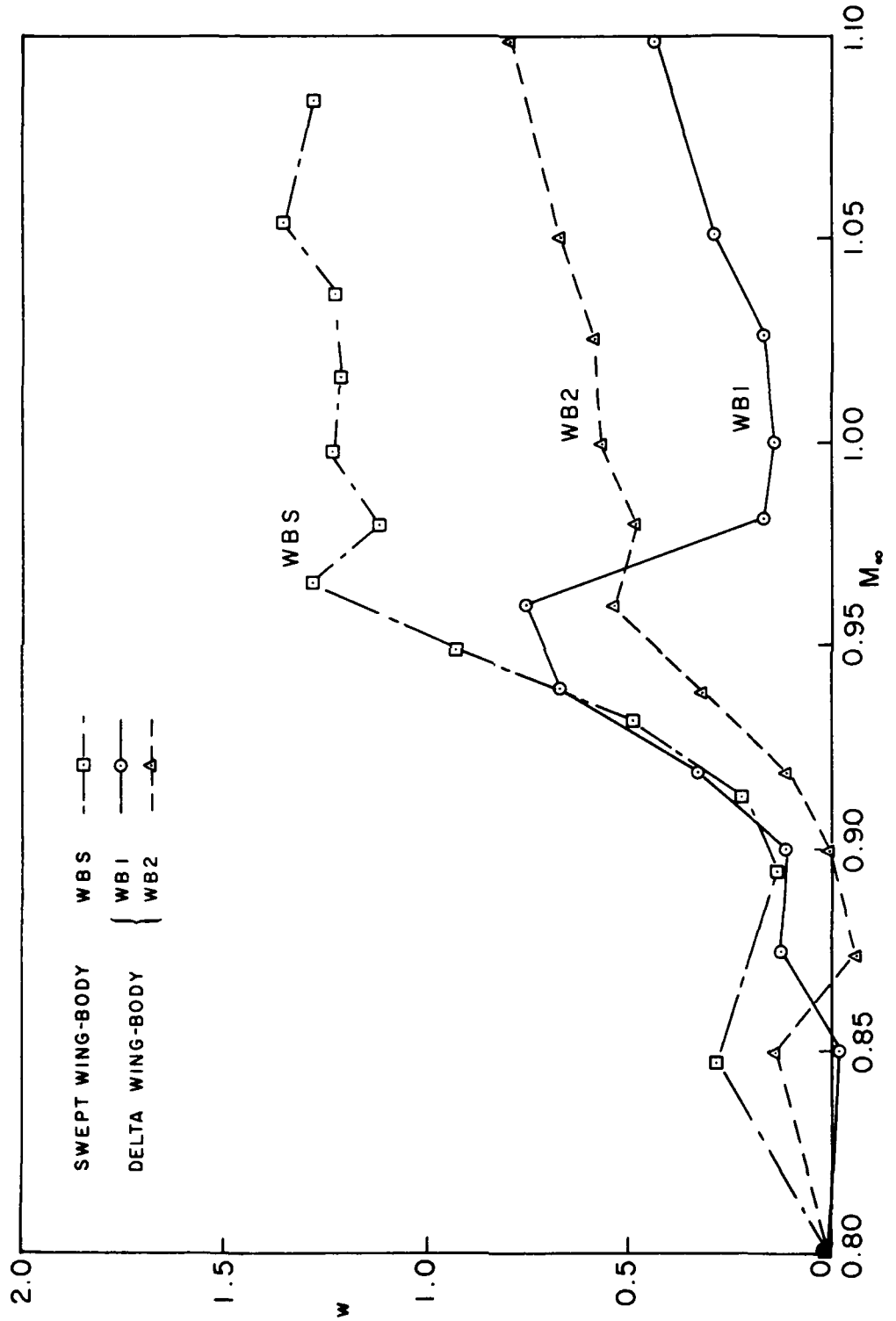

FIG. 14: VARIATIONS OF WAVE DRAG FACTOR k_w WITH MACH NUMBER FOR SWEPT WING AND DELTA WING MODELS

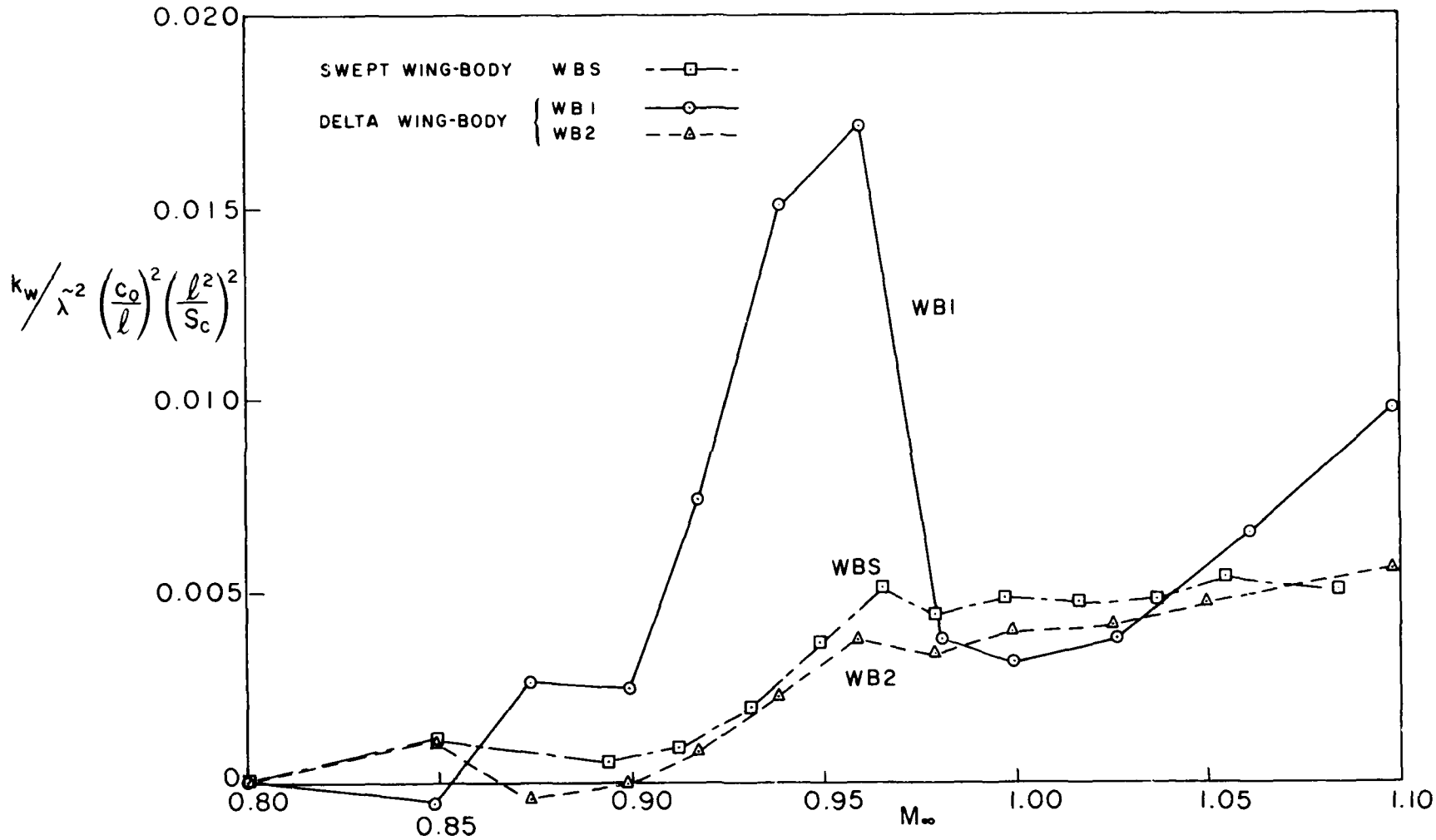

FIG. 15: CORRELATIONS OF WAVE DRAG FACTOR k_w WITH MACH NUMBER FOR FIXED LIFT PARAMETER $\tilde{\epsilon}\frac{\tilde{\alpha}}{\tilde{\tau}}$

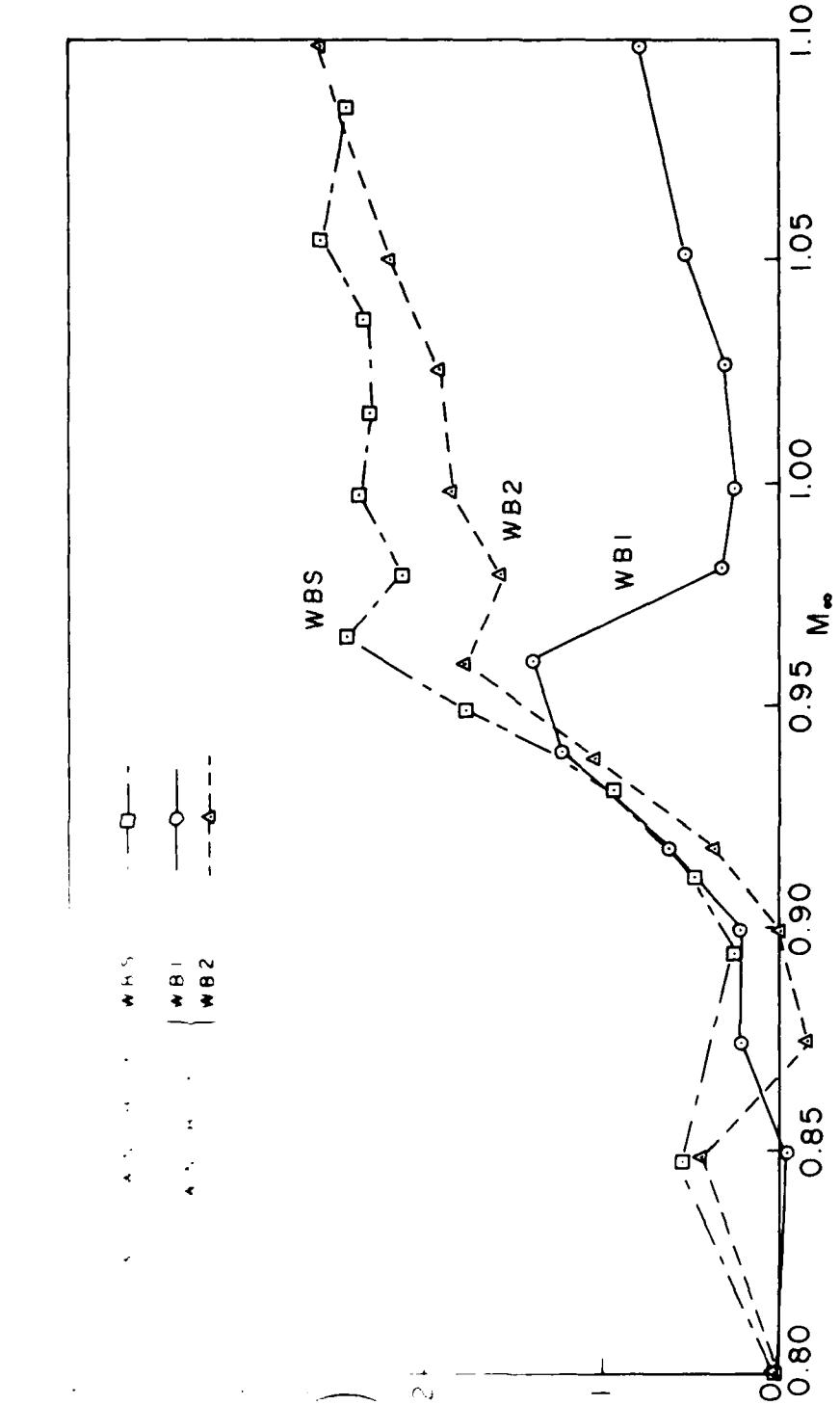

FIG. 16: CORRELATIONS OF WAVE DRAG FACTOR k_w WITH MACH NUMBER FOR FIXED LIFT COEFFICIENT C_L^2/A

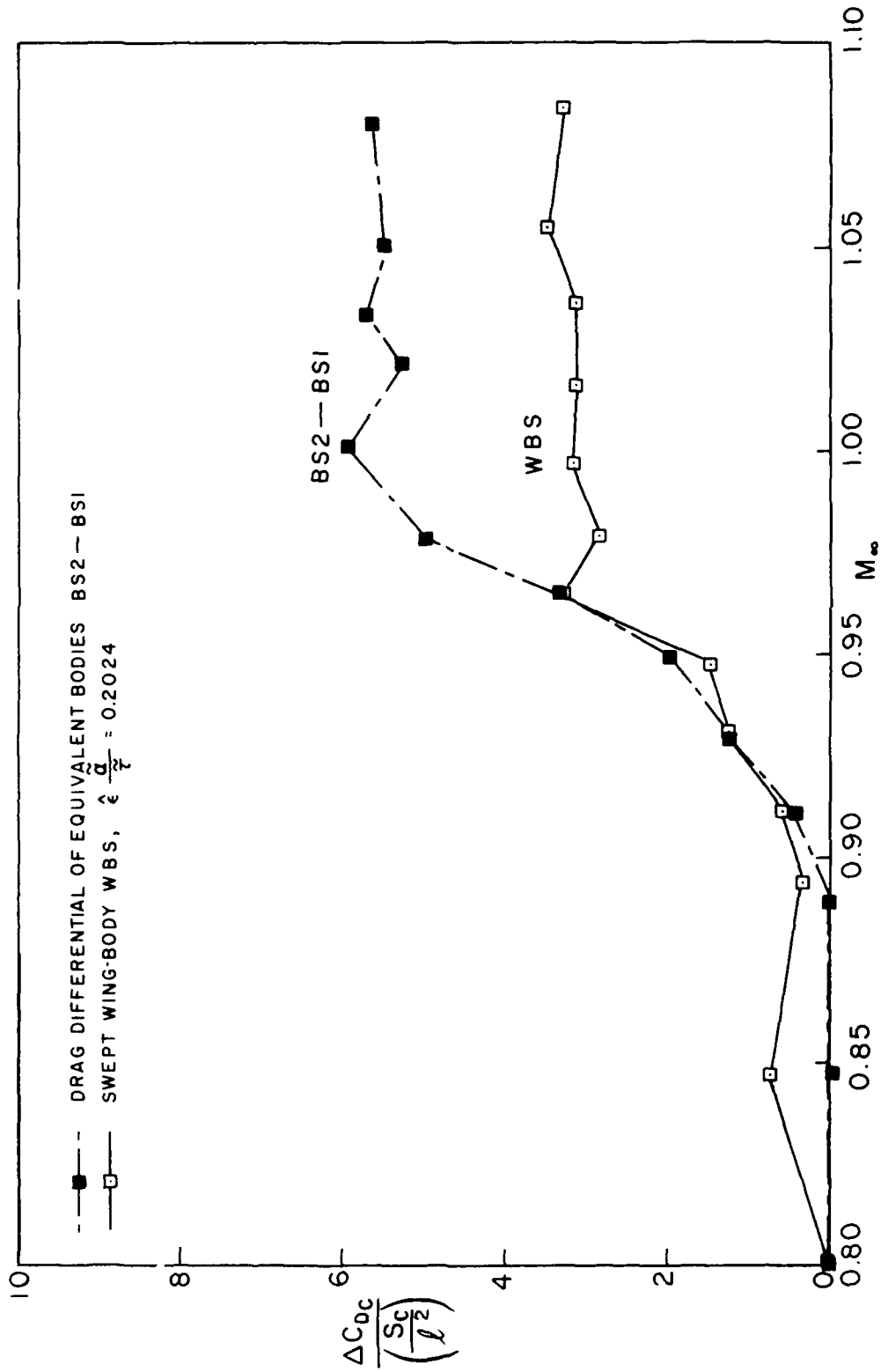

FIG. 17: COMPARISON OF DRAG-RISE DUE TO LIFT FOR SWEPT WING-BODY WBS AND DRAG-DIFFERENTIAL OF EQUIVALENT BODIES BS2–BS1

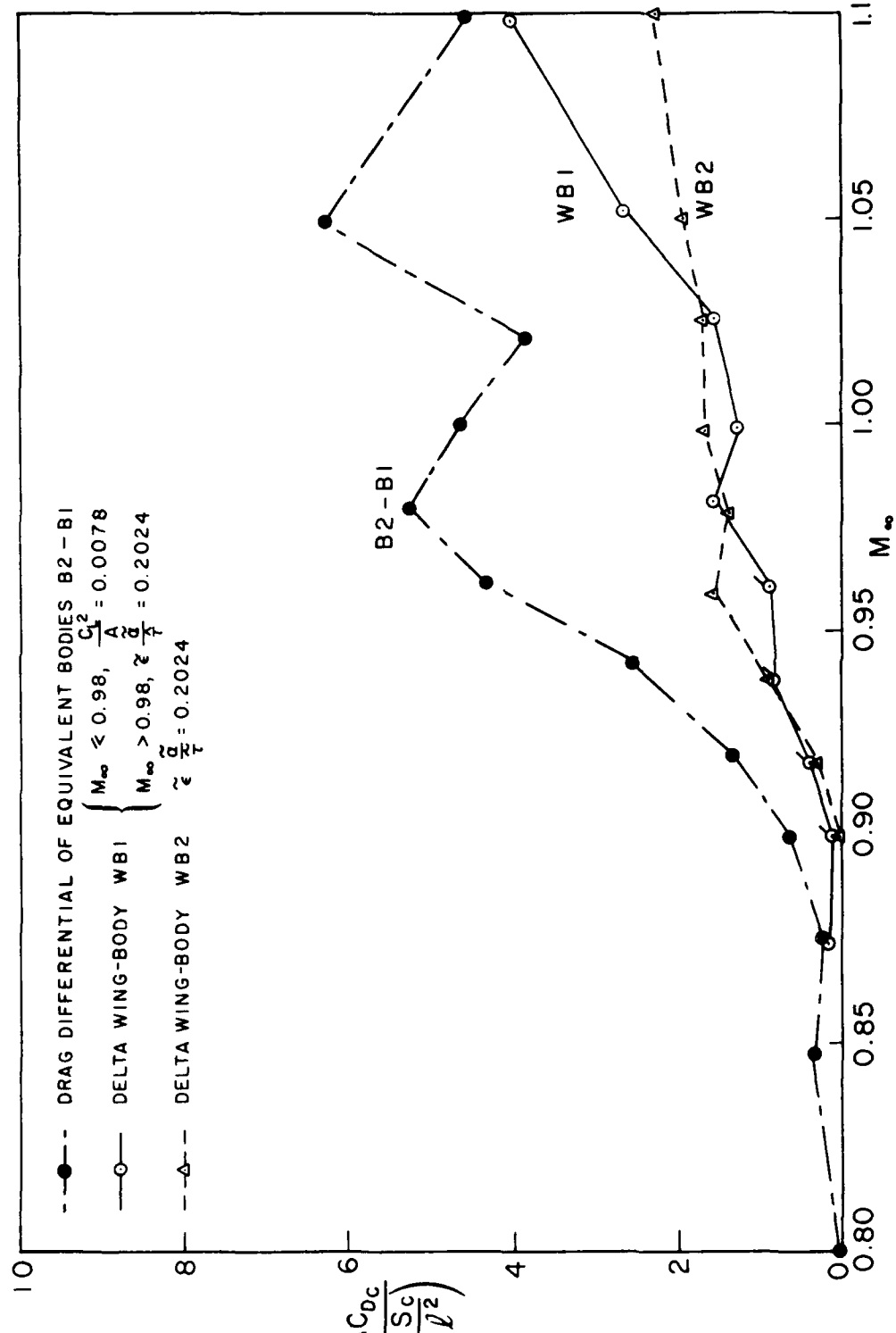

FIG. 18: COMPARISON OF DRAG-RISE DUE TO LIFT FOR DELTA WING-BODIES WB1, WB2 AND DRAG-DIFFERENTIAL OF EQUIVALENT BODIES B2–B1

APPENDIX

EVALUATION OF FUNCTIONS T(x), E(x) AND F(x) FOR A SWEPT WING

The functions F(x), T(x) and E(x) constitute the expression for the effective area due to lift (Eq. (10) in the text). All involve integrations in the y-direction and both T(x) and E(x) involve double integrals. These integrals are evaluated numerically as follows.

The function T(x) has the form (Eq. (6) of Ref. 1)

$$T(x) = \frac{1}{4\pi} \int_{a_1}^{a_2} \int_{a_1}^{a_2} [\![\phi(x,s)]\!]_x \; [\![\phi(x,y)]\!]_x \; \ell n \frac{1}{|y-s|} \, dsdy \tag{A1}$$

where a_1 and a_2 are the y-co-ordinates of the leading edges for each side of the wing respectively. The integrals can be evaluated in sequency as

$$T(x) = \frac{1}{4\pi} \int_{a_1}^{a_2} [\![\phi_x(x,y)]\!] \left(\int_{a_1}^{a_2} [\![\phi_x(x,s)]\!] \ell n \frac{1}{|y-s|} \, ds \right) dy \tag{A2}$$

As x appears only as a parameter, the integrands are now written without x and the square bracket for short. For the integral with respect to s the integrand $\phi_x(s)$ is written for the integral Δs by the trapezoidal rule as

$$\begin{aligned} \phi_x(s) &= \phi_{x_n} + \frac{\phi_{x_{n+1}} - \phi_{x_n}}{s_{n+1} - s_n} (s - s_n) \\ &= \phi_{x_n} - \phi^n_{x_s} s_n + \phi^n_{x_s} s \end{aligned} \tag{A3}$$

where

$$\phi^n_{x_s} = \frac{\phi_{x_{n+1}} - \phi_{x_n}}{s_{n+1} - s_n}$$

and

$$\Delta s = s_{n+1} - s_n = \frac{a_2 - a_1}{N - 1}$$

Substituting Equation (A3) into Equation (A2) and evaluating the integrals, we have

$$I(y) = - \sum_{n=1}^{N-1} \left[\left(\phi_{x_n} - \phi^n_{x_s} s_n \right) I_{1n}(y) + \phi^n_{x_s} I_{2n}(y) \right] \tag{A4}$$

where

$$I_{1n}(y) = \left[(y - s_{n+1}) \ln |y - s_{n+1}| - (y - s_n) \ln |y - s_n| + (s_{n+1} - s_n)\right]$$

$$I_{2n}(y) = 1/2\left[(y^2 - s_{n+1}^2) \ln |y - s_{n+1}| - (y^2 - s_n^2) \ln |y - s_n| + y(s_{n+1} - s_n) + 1/2(s_{n+1}^2 - s_n^2)\right]$$

The integral with respect to y can then be written with the trapezoidal rule as

$$T(x) = \frac{1}{4\pi} \sum_{m=1}^{M} \left\{ \left[\phi_x(y)I(y)\right]_{m+1} + \left[\phi_x(y)I(y)\right]_m \right\} \frac{y_{m+1} - y_m}{2} \qquad (A5)$$

It is explicit that $s_n \neq y_m$ for n = m.

The function E(x) has the form (Eq. (7) of Ref. 1)

$$E(x) = \frac{1}{4\pi} \int_{a_1}^{a_2} \int_{a_1}^{a_2} [\![\phi(x,y)]\!]_y [\![\phi(x,s)]\!]_y \ln \frac{1}{(y - s)} \, dsdy \qquad (A6)$$

and can be evaluated in the same way as T(x) with $[\![\phi_y(x,y)]\!]$ replacing $[\![\phi_x(x,y)]\!]$.

The function F(x) involves a single integral (Eq. (5) of Ref. 1)

$$F(x) = \int_{a_1}^{a_2} [\![\phi]\!] dy \qquad (A7)$$

In calculating the effective area due to lift, the x-derivative of F(x) is used. Again applying the trapezoidal rule, the $F_x(x)$ can be written as

$$F_x(x) = \sum_{m=1}^{M} \left[\phi_{x_{m+1}} + \phi_{x_m} \right] \frac{y_{m+1} - y_m}{2} + \phi(x,a_2) \frac{da_2}{dx} - \phi(x,a_1) \frac{da_1}{dx} \qquad (A8)$$

For a fixed x station, the numerical procedure is carried out along the y-direction from $a_1(x)$ to $a_2(x)$ over the wing and the wake. The velocity potential and its derivatives are given in Equations (4), (5) and (6) over the wing, Equations (7), (8) and (9) for the wake. The resulting functions are shown in Figure 3.

REPORT DOCUMENTATION PAGE / PAGE DE DOCUMENTATION DE RAPPORT

REPORT/RAPPORT LR-614 1a	REPORT/RAPPORT NRC No. 23412 1b
REPORT SECURITY CLASSIFICATION CLASSIFICATION DE SÉCURITÉ DE RAPPORT Unclassified 2	DISTRIBUTION (LIMITATIONS) Unlimited 3

TITLE/SUBTITLE/TITRE/SOUS-TITRE

An Experimental Study of the Transonic Equivalence Rule with Lift
Part II

4

AUTHOR(S)/AUTEUR(S)

Y.Y. Chan

5

SERIES/SÉRIE

Aeronautical Report

6

CORPORATE AUTHOR/PERFORMING AGENCY/AUTEUR D'ENTREPRISE/AGENCE D'EXÉCUTION

National Research Council Canada
National Aeronautical Establishment — High Speed Aerodynamics Laboratory

7

SPONSORING AGENCY/AGENCE DE SUBVENTION

8

DATE	FILE/DOSSIER	LAB. ORDER COMMANDE DU LAB.	PAGES	FIGS/DIAGRAMMES
84-03			45	18
9	10	11	12a	12b

NOTES

13

DESCRIPTORS (KEY WORDS)/MOTS-CLÉS

1. Wings (swept-back)
2. Wings (delta)
3. Transonic equivalence rule

14

SUMMARY/SOMMAIRE

The experimental study of the transonic equivalence rule with lift, previously reported in Reference 1, has been extended to include a configuration of swept-back wing-body and the corresponding equivalent bodies for lift and zero-lift. For zero lift, the wing-body is shown to have higher wave drag than that of the equivalent body. At lifting condition, the analyses of the data, including those of the delta wing-bodies reported in Reference 1, have verified the similitude of drag rise due to lift between the wing-bodies. The additional drag induced by the effective area due to lift on the equivalent body was found to agree reasonably with the wave drag generated by lift on the wing-body. The experiment thus verified the area rule with lift which must be considered in the optimal design of transonic configurations.

15